2018

Modelling and Analysis of Chevy Volt Gen II Hybrid Vehicle in Electric Mode

Kaushik Surresh
Michigan Technological University, ksurresh@mtu.edu

MODELLING AND ANALYSIS OF CHEVY VOLT GEN II HYBRID VEHICLE IN ELECTRIC MODE

By

Kaushik Surresh

A REPORT

Submitted in partial fulfillment of the requirements for the degree of

MASTER OF SCIENCE

In Mechanical Engineering

MICHIGAN TECHNOLOGICAL UNIVERSITY

2018

This report has been approved in partial fulfillment of the requirements for the Degree of MASTER OF SCIENCE in Mechanical Engineering.

Department of Mechanical Engineering- Engineering Mechanics

Report Co-Advisor:	*Dr. Mahdi Shahbakthi*
Report Co-Advisor:	*Dr. Darrell Robinette*
Committee Member:	*Dr. Bo Chen*
Department Chair:	*Dr. William Predebon*

Table of Contents

List of figures

List of tables

Acknowledgments:

I would like to express my gratitude and thanks to Dr. Mahdi Shahbakthi and Dr. Darrell Robinette for providing me an opportunity to work on this project. Their constant guidance, support and feedback were fundamental in helping me complete my project. I would like to thank Dr. Bo Chen for being a part of my defense panel. A special thanks to all NextCar project members especially Rajeshwar Yadav who helped a lot with my work. I would like to acknowledge the support of my friends and faculty who have instrumental in my Master's education. Finally, I would like to thank my parents to whom I owe everything

List of abbreviations:

ANL -	Argonne National Labs
GM -	General Motors
TPIM -	Traction Power Inverter Module
EV -	Electric Vehicle
HEV -	Hybrid Electric Vehicle
PHEV -	Plug-in Hybrid Electric Vehicle
EREV -	Electric Range Extended Vehicle
GHG -	Greenhouse Gases
CD -	Charge Depleting
UDDS -	Urban Dynamometer Driving Schedule
HWFET -	Highway Fuel Economy Test
LDV -	Light-duty vehicle
SOC -	State of Charge
OCV -	Open Circuit Voltage
R-C -	Resistance Capacitance
MG A -	Motor Generator A
MG B -	Motor Generator B
OWC -	One Way Clutch
LVD -	Longitudinal Vehicle Dynamics

List of Symbols

T	-	Temperature (K)
R	-	Resistance (Ω)
I	-	Current (A)
V	-	Voltage (V
I	-	Moment of Inertia
R	-	Radius of Ring gear
S	-	Radius of Sun gear
ω	-	Angular Speed
$\dot{\omega}$	-	Angular Acceleration
c_p	-	Heat Capacity
F	-	Force (N)
V	-	Velocity(m/s)
M	-	Mass (Kg)

Abstract

The technical report discusses the high-fidelity modelling of the powertrain of Chevy Volt Gen II Hybrid Vehicle in the Electric Mode. The objective of the powertrain model was to predict total energy consumed within 5% of experimental data for different drive cycles in Charge Depleting Mode. The following powertrain elements were modelled in Matlab and Simulink using parameters and performance maps provided by General Motors: battery, E-Motor, TPIM power electronics, transmission auxiliary pumps, spin losses, drive unit and vehicle dynamic models. The report discusses the development of each of the powertrain components and development of the EV supervisory controller which commands the EV modes and motor torques from the vehicle speeds inputs

The overall powertrain model was validated for three drive cycles in Charge Depleting (EV) mode i.e. HWFET, UDDS, US06 based on test data provided by Argonne National Lab. The model predicts the total battery energy consumption with errors less than 5% for the three drive cycles. An analysis of energy consumption in vehicle and the source of errors is presented.

1 Introduction

The technical report focusses on the modelling of Chevy Volt Powertrain in EV mode as a part of the NextCar Project. A brief introduction about the project goals and an in-depth discussion of the modelling exercise is provided in this report. The flow of the report is given below.

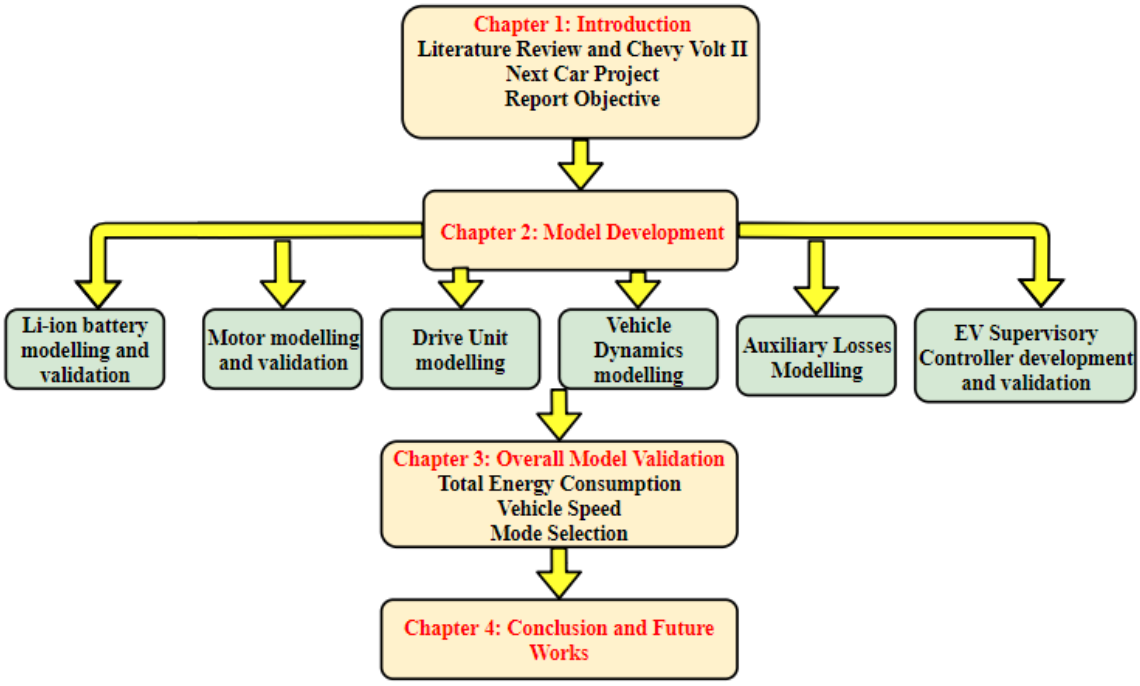

Figure 1. Structure of Report

Chapter 1 deals with the general trends in the automotive industry for Hybrid Electric Vehicles, a brief description of Chevy Volt Gen II which is chosen for study in this report, the motivation behind the NextCar project and how this work helps in addressing some of the project objectives and a literature review of modelling approaches used.

Chapter 2 discusses the modelling of different subsystems of Chevy Volt model and its validations. Chapter 3 presents the validation of the overall integrated model and final results. Chapter 4 provides the conclusion and future scope of this modelling work.

1.1 General trends of Hybrid Electric Vehicles

Strict legislation regarding emissions and fuel economy and increasing consumer awareness regarding environmental pollution has led to auto manufacturer push towards electrification of their powertrains since they are an effective measure to reduce

greenhouse gas emissions and fuel consumption. Corporate Average Fuel Economy Standards(CAFÉ) dictate that Light Duty Vehicles have to achieve 54.5 mpg by the model year 2025[1]. It becomes important to focus on the Light Duty Vehicles since they occupy a greater portion of the production share(figure 2) and contribute about 60% GHG emissions of the transportation sector[2]

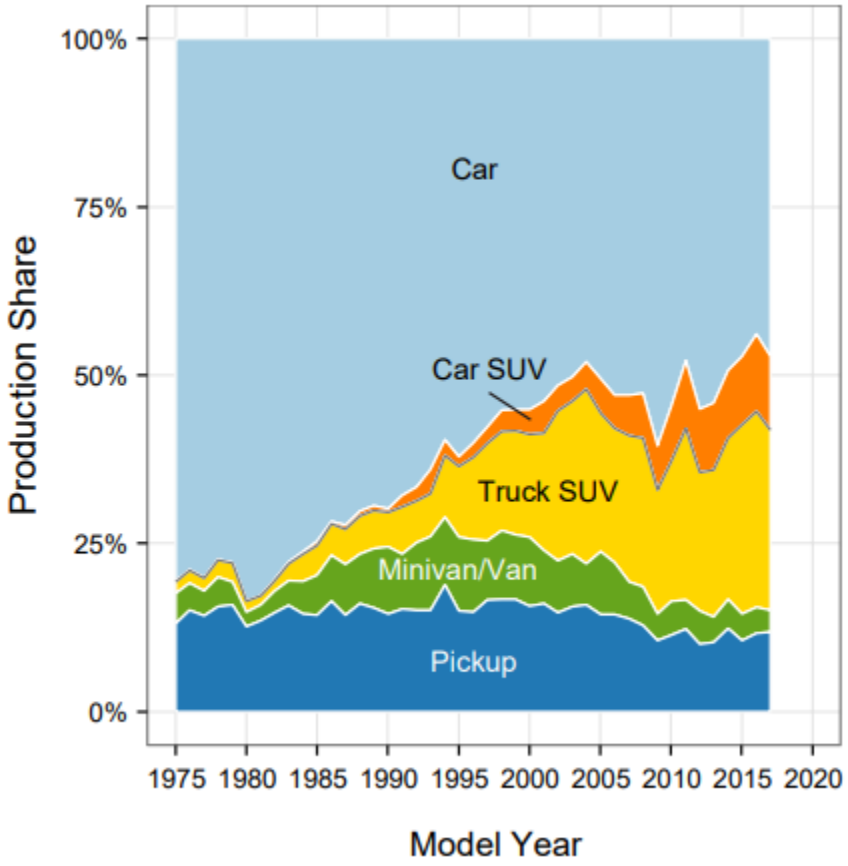

Figure 2. Production share of Light-duty vehicles [3]

Auto Manufacturers have adopted various technologies like Gasoline Direct Injection, Turbocharging, lean combustion strategies, cylinder deactivation, valve timing and lower friction lubricants etc. Electrification of powertrains also feature among their plans

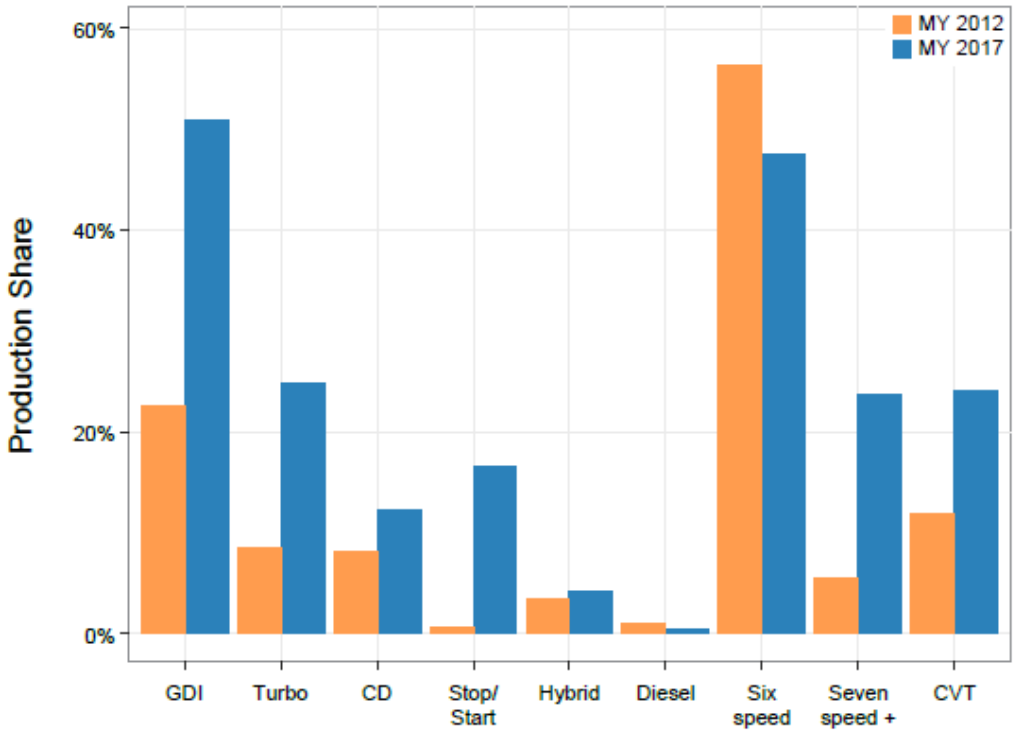

Figure 3. Production Share of different technologies in MY 2012 and 2017 comparison [3]

.

Figure 3 above shows how the manufacturers have adopted different technologies for meeting fuel economy and emission standards over the model years 2012 and 2017. Among electrification strategies, the production of HEV (strong) increased only slightly whereas the start/stop hybrid system (mild hybrids) production increased drastically from 2012 to 2017. Mild electrification provides much of the benefits with lower costs and hence its adoption rates improved drastically over the years. But to meet the future ambitious targets set by CAFÉ it is imperative that manufacturers shift to completely electric vehicles or strong hybrids in their vehicle lineup.

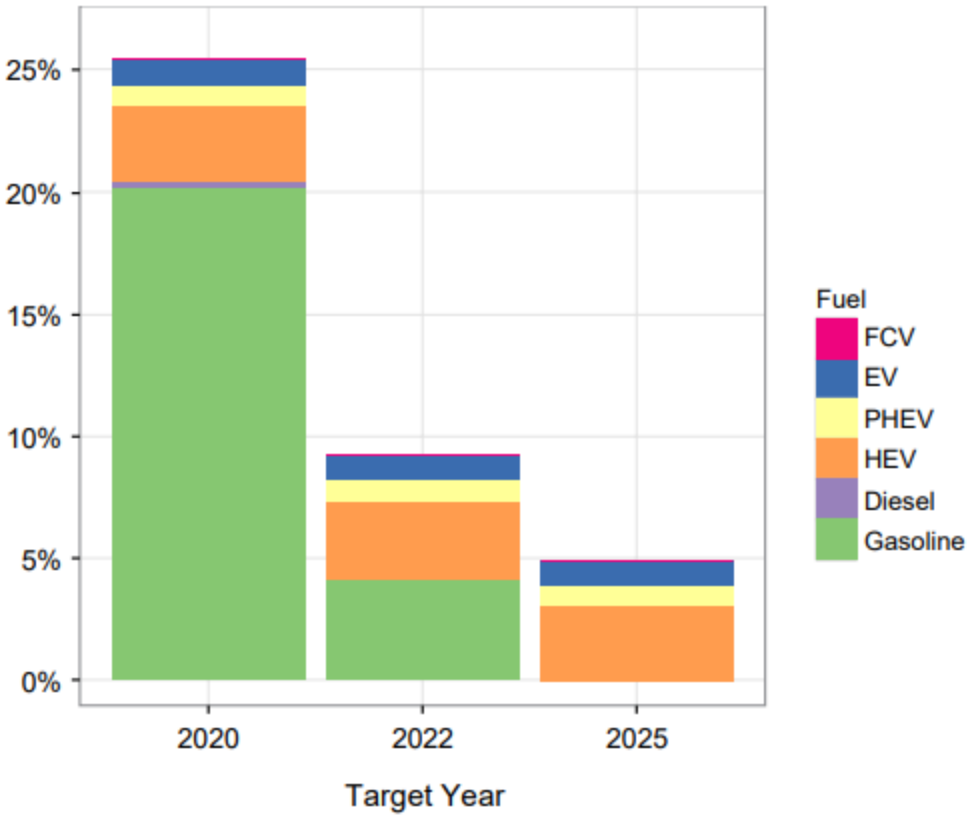

Figure 4. Percentage of MY 2017 vehicles which meet 2020, 2022 and 2025 CAFE standards[3]

Figure 4 shows the percentage of MY 2017 vehicles which meet CAFÉ standards in 2020, 2022 and 2025. It is to be noted for MY 2025 for light-duty vehicles only the alternate vehicles of MY 2016 (HEV, EV, PHEV, FCV) could meet the targets. Though gasoline/diesel technologies could be further refined to meet the targets the necessity of the electrified powertrains becomes imperative in the future. Thus it is necessary for the automaker to concentrate the better portion of the research on alternative fuel vehicles. Among the alternative fuel vehicles HEV, PHEV, EREV and BEV feature prominently. The main deterrent to higher electrification of powertrains remains the battery sizing and costs to maintain the same vehicle performance.

HEV achieve fuel consumption reduction compared to conventional powertrains through engine downsizing, regenerative braking and reducing idle and operating the downsized engine at its most efficient operating point [4]. HEV powertrain architecture is of three types: series, parallel and power split with each having its characteristic advantages and driving dynamics. Plug-in Hybrid Electric Vehicles represent a step above conventional HEV in terms of electrification. According to a formal definition, they should have provision to recharge the battery from an external source, have battery energy of at least 4KWh and should have an all-electric range of at least 10 miles.[5] Battery electric vehicles solely rely on the battery for propulsion. Small vehicles for urban driving seem

most suited to BEV due to low driving range. However companies like Tesla release Type C and D vehicles (sedans) BEV with larger battery packs and have received considerable welcome.

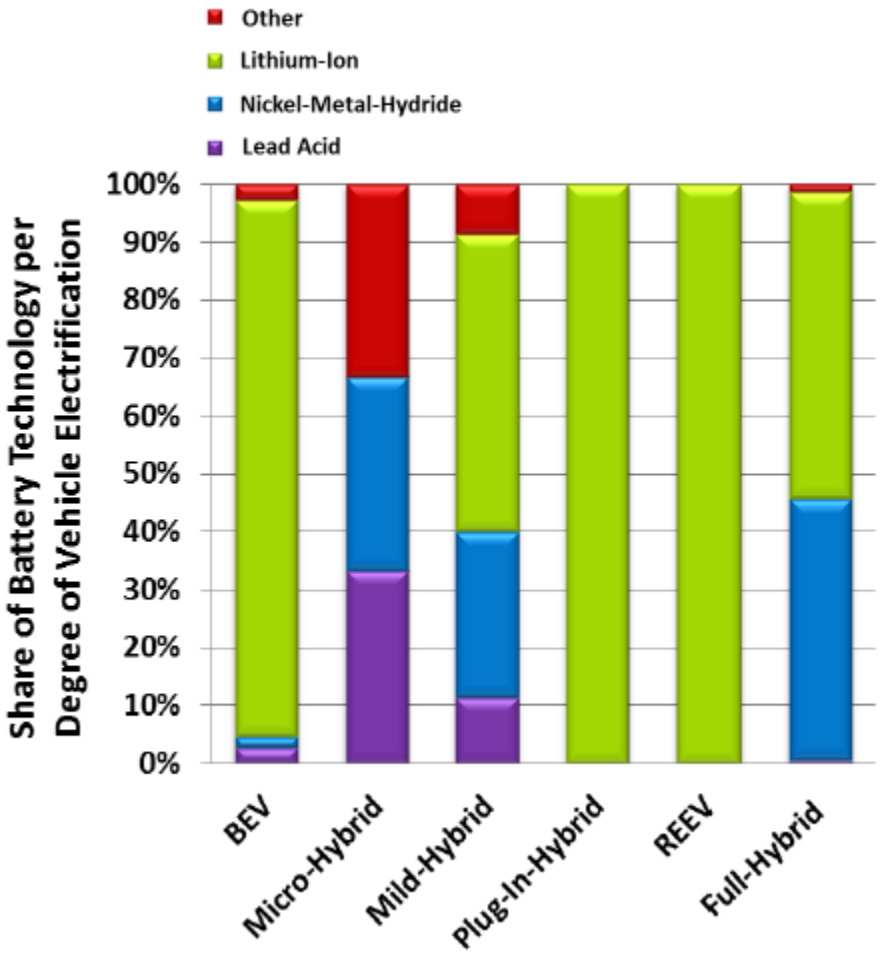

Figure 5. Share of different battery chemistries under varying electrification stages [6].

From figure 5 we can infer that the as the degree of electrification increases Li-ion battery chemistry is preferred because of its higher energy density, low self discharge and memory characteristics. Among the E-machines polyphase motor with permanent magnets made up of rare earth metal is widely used because of its high power density, efficiency and compactness. Because of the rising cost of such rare earth metals research is focused on other types of externally excited motors like switched reluctance, induction motors and measures to reduce the usage of rare earth metals.

In addition to electrification digitization is expected to provide major transformation in transportation sector and redefine personal mobility through technologies like connected vehicles, Internet of things and autonomous vehicles. [7].

1.2 Chevy Volt Gen II:

The Chevy Volt Generation 2 (GEN 2) model was released in 2016 as an improved version of Chevy Volt Gen 1 Range Extended Vehicle. The Generation II vehicle was designed from a fresh design perspective incorporating the experiences and feedback from Gen I vehicle. The GEN 2 model had among the improvements better electric range, better fuel economy in Charge Sustaining mode and better performance characteristics.

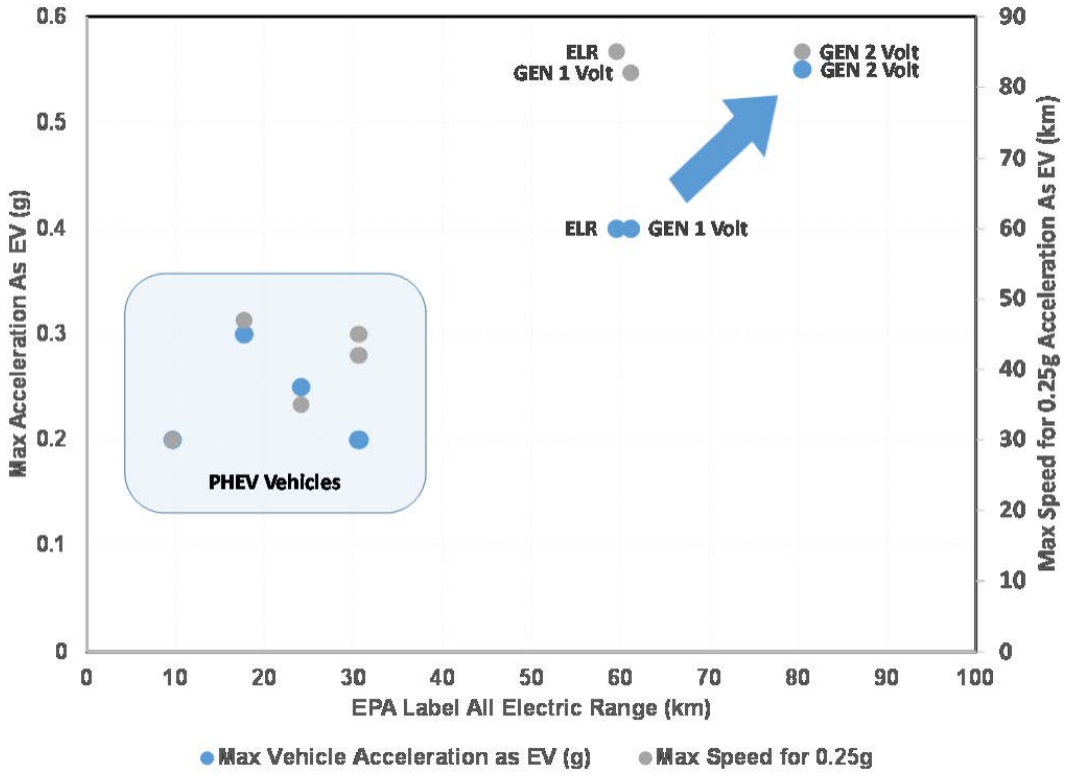

Figure 6. Improved electric range and performance of Chevy Volt GEN 2[8]

Figure 8 shows the benchmarking of Chevy Volt Gen II performance characteristics against Gen I and other hybrid electric vehicles in the market. Chevy Volt has better maximum acceleration and all-electric range comparatively.

One of the major changes is split of EV propulsion among two Motor generators (MG-B and MG-A) in which MG-B meets the majority of the torque demands and MG-A assisted MG-B at high torque requirements. The strategy of multi-mode EV propulsion resulted in increased efficiency and smoother vehicle starting. Due to power split among

the motor the motor torque/power requirements reduced, motor operational efficiency improved and enabled a reduction in motor volumes and bearing sizes [8]. Also, the use of rare earth materials in the Motor B is reduced by Grain Boundary Dysprosium Diffusion process and eliminating rare earth elements in Motor A by ferrite magnets since Motor A is used sparingly [9]. Since Motor A operated at zero torques mostly using a ferrite which has weaker magnetic flux help reduce speed-related losses.

Better selection of planetary gear and final drive ratios and decision to split EV propulsion contributed to volume and mass reductions of 20 and 40% respectively. Also because of lower torque and power limits in the motor and better cooling configurations the inverter sizes could be reduced and integrated to the transaxle assembly which eliminates the volume that would have been occupied by the high voltage 3-phase AC cables.

Some of the important technical changes to the battery system are summarized below

Table 1. Chevy Volt Gen 1 vs Gen 2 Battery Specs

Technical Specification	**Gen 1 Volt**	**Gen 2 Volt**
Cell Configuration	96 S 3P(288 Cells)	96S 2P (192 cells)
Discharge Power	110 KW	120 KW
Usable Energy	10-11.2 KWh	14 KWh
Total Energy	16-17.1KWh	18.4 KWh
Energy Density-Volume	118 Wh/l	119 Wh/l
Energy Density-Mass	87 Wh/kg	101 Wh/kg
Mass	196 kg	183 kg
Module Sizes	18*36 cells	24*32 cells

The noticeable gains from the previous generation include an increase in total energy capacity by 12%, higher discharge power, usable and total energy even-though the cell

chemistry remains the same. The cell configuration has been changed from 3 cells to 2 cells in parallel. This helped in better packaging efficiency and helped achieve higher energy density (mass and volume) [8]. Apart from the improvements to the primary propulsion system components reductions in brake drag, accessory loads and better charging systems were designed.

1.2.1 Operating Modes of Chevy Volt Gen II

Based on the torque request and vehicle speed, the two planetary gear sets and three clutches are engaged accordingly to result in the following five operation modes for the vehicle

i. One Motor EV: An all-electric mode in which MG-B alone propels the vehicle at low power requests
ii. Two Motor EV: An all-electric mode in which both MG-A and MG-B provide the traction power requirements while regenerative braking is through MG-B.
iii. Low Extended Range (LER): A Charge sustaining mode in which both MG-B and engine provides the traction power requirements. A portion of energy provided by the engine is converted to electrical energy by MG-A to recharge the battery.
iv. Fixed Ratio Extended Range (FER): A charge sustaining mode in which both engine and MG-B is used to propel the vehicle at intermediate power request
v. High Extended Range (HER): A charge sustaining mode in which engine, MG-A and MG-B propel the vehicle at peak power requests.

1.3 NextCar Project:

The modelling work in this report is undertaken based on the 'NEXT Generation Energy Technologies for Connected and Automated On-Road Vehicles' i.e. NextCar Project funded by Department of Energy (DOE). The project aims to leverage the connectivity and automated driving technologies to optimize powertrain and vehicle dynamics operation and help in reducing the energy consumption of the future fleet. Features like vehicle to vehicle and vehicle to infrastructure communication provide information related to future driving condition like a traffic stop or downward slope. By anticipating the future driving conditions, we can optimize the vehicle (acceleration, braking) and powertrain actions (engine operating point, regenerative braking and battery management) to reduce the energy consumption. Through such optimized actions, the program has a target of reducing the energy consumption of future vehicles by 20%

Michigan Technological University in partnership with General Motors aims to demonstrate energy efficiency improvements in hybrid vehicle platoon using advanced controls and mobile cloud computing. The hybrid vehicle chosen is the Chevy Volt Gen

II PHEV. Using information from vehicle connectivity, real-time traffic simulation and eco-routing, a Model Predictive Controller is used to optimize the vehicle dynamic and powertrain operation and demonstrate improvements on a fleet of 8 Chevy Volts. A 20 % reduction in energy consumption can result in 8% improvements in range for future hybrid electric vehicles.

1.3.1 Report Objective:

A powertrain model for accurately predicting the vehicle energy consumption is required by the Model Predictive Controller to optimize vehicle actions. Thus, the objective is to develop a powertrain model that can predict energy consumption with errors less than 5%. This report addresses the powertrain model development of Chevy Volt Gen 2 vehicle in the electric mode. The model development for individual powertrain components, their validation and integrated model validation has been discussed in this report.

The model development was achieved through a combination of dynamic models from literature and using maps obtained from experimental testing. The parameters for dynamic models and the maps have been provided by GM. The model was built in Matlab/Simulink programming system. The validation of the model was carried out by comparing with vehicle test data provided by ANL.

1.4 Modelling Approaches Literature Review:

HEV powertrain is a complex system consisting of numerous components like the electrical energy storage, IC engines, hydraulic components etc. To ensure good fuel economy and drivability it is important to characterize the dynamic interactions among the components and choose optimum designs. Physical prototyping and testing can prove to be very expensive in understanding the design consideration. Hence modelling and simulation play an important role in HEV powertrain design and analysis [10].

Based on the level of details in modelling of components vehicle models can be classified as steady state, dynamic and quasi-static. Steady-state models and quasi static models typically use map-based models of vehicle sub-systems. Their main advantage is quick computation time but since they do not consider system dynamics they become inaccurate for transient operations. Examples of steady-state vehicle modelling packages include Autonomie[11][12][13] and ADVISOR[14]developed by ANL and NREL respectively. Example of quasi-static vehicle modelling package is the Powertrain System Analysis Toolkit (PSAT) developed by ANL [15]. Dynamic modelling approach used physics-based models for vehicle subcomponents thereby ensuring good accuracy in transient conditions. Examples of such dynamics vehicle models have been dealt with in works [16][17][18].

Vehicle models are further classified as forward or backward models depending on the direction of calculation. [19]. Forward models also called the rear to front model begins the calculations of quantities at the primary energy source i.e. the engine or the electrical energy storage. PSAT is one kind of forward model. The calculation proceeds in the forward direction of powertrain power flow using transmitted torque and reflected torque. This model needs a driver model like a PID controller for speed control. Another class of models named backward models work from the traction force request at wheels to the primary energy source and is generally made of quasi-static models. ADVISOR is one example of backward model. The modelling work undertaken in this project can be considered as a hybrid static-dynamic model which works based on the backward approach. The drive cycle velocity is used to determine the tractive forces and works its way backward towards the primary energy source i.e. to calculate the battery electrical energy required for the drive cycle maneuver.

2 Modelling

The Modelling section describes in detail about each of the subsystems of Chevy Volt powertrain model

2.1. Overview

The drive cycle speeds are taken as inputs ANL experimental data and the model predicts the total electrical energy consumed and the battery SOC. A PI controller and rule-based control logic are used to predict the torque request and blending ratio between MGA and MGB respectively. The rule-based control logic was extracted by analysis of the experimental data provided by ANL.

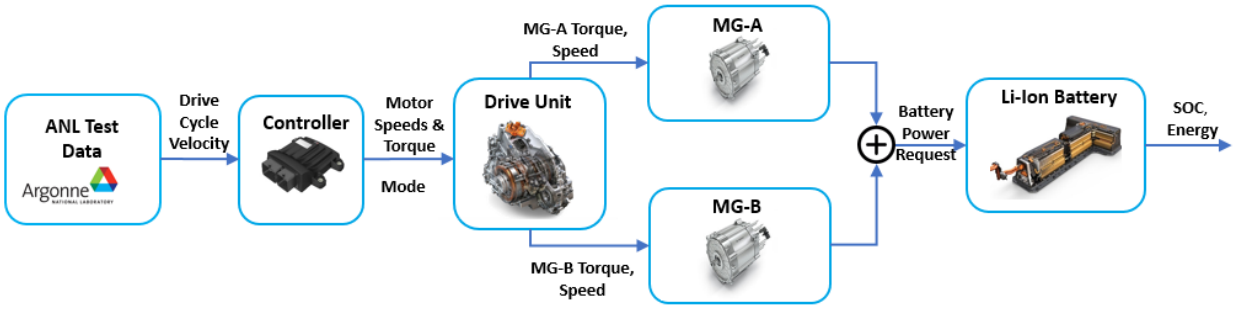

Figure 7. Model Overview

2.2. Battery

Chevy Volt Gen II uses a 18.4 kWh battery pack composed of 96 cells in 2 cell parallel configuration. The cells of Li-NMC battery chemistry pouch type cells. At high temperatures, the battery is managed thermally by an active liquid cooling system. Compared to Gen I battery the Gen II battery pack has higher total energy, energy density and usable power

2.2.1. Battery Electric Model:

A dynamic electric model of the Li-ion battery based on the Equivalent Circuit Method has been developed[20]. In literature, there exist different kinds of equivalent circuit models starting from the simple Rint model which consists of an Open circuit voltage source and internal resistance. For highly dynamic loads such ones experienced by an HEV it does not capture the dynamics accurately. For this purpose, various models such as simple R-C, PNGV, Thevenin models utilize an R-C circuit to capture the dynamics caused by polarization[25]. Two R-C circuit model or dual polarization battery model is an improved version of Thevenin model with an extra RC circuit to capture the dynamics

caused by difference in electrochemical and concentration polarization at the end of the charging or discharge cycles. Among the class of models two R-C circuit models with accurate parameters estimation are most accurate for SOC predictions and dynamic test performance[26]. Hence it is adopted to model the Li-ion battery pack of Chevy Volt. The battery is modelled as two circuit linked by a voltage controlled voltage source and a current controlled current source. Figure 3 below shows the schematic of the equivalent electric circuit of the Li-ion battery.

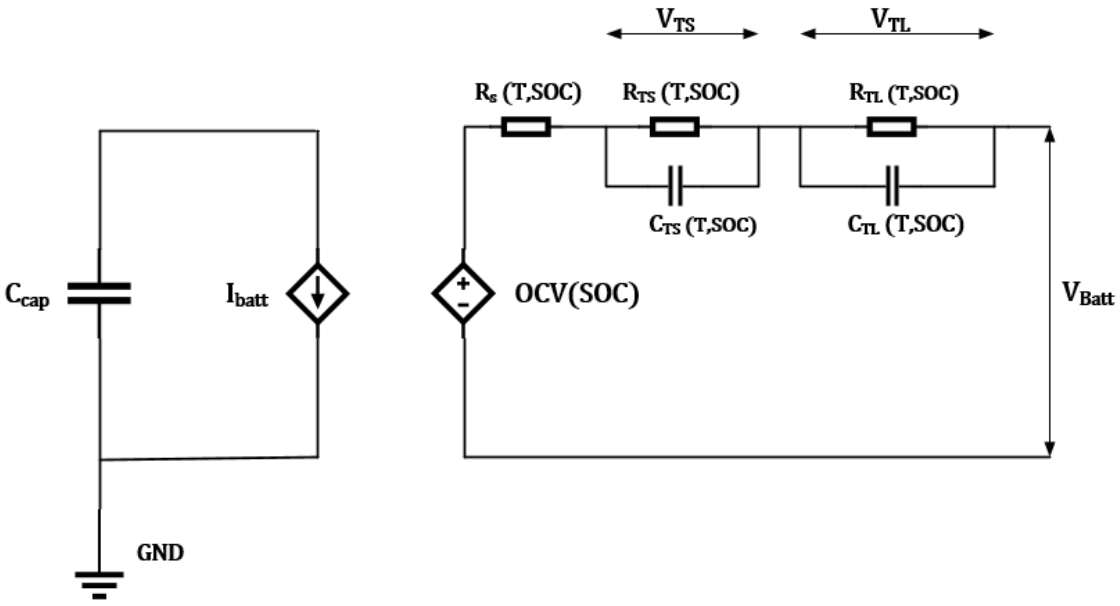

Figure 8. Battery Electrical Circuit Diagram

$$P_{batt} = V_{batt} * I_{batt} \quad (1)$$

$$\frac{dV_{CTS}}{dt} = \frac{-V_{CTS}}{R_{TS}C_{TS}} - \frac{i_{batt}}{C_{TS}} \quad (2)$$

$$\frac{dV_{CTL}}{dt} = \frac{-V_{CTL}}{R_{TL}C_{TL}} - \frac{i_{batt}}{C_{TL}} \quad (3)$$

$$V_{batt} = OCV + V_{CTS} + V_{CTL} + R_s . i_{batt} \quad (4)$$

$$SOC = SOC_O - \int \frac{i_{batt} dt}{Q} \quad (5)$$

V_{CTS}, R_{TS}, C_{TS} represent the voltage drop, resistance and capacitance of the shorter time constant R-C circuit.

V_{CTL}, R_{TL}, C_{TL} represent the voltage drop, resistance and capacitance of the longer time constant R-C circuit.

OCV is the open circuit voltage of the battery which is dependent on SOC and R_s is the internal resistance of the battery.

The circuit on the left models the overall charge capacitance of the battery. The right side circuit models the battery internal resistance and the dynamics of battery though a series resistance and a network of 2 R-C Circuits. The voltage controlled voltage source represents the non-linear relationship between OCV and SOC. Figure 4 below shows the outline of battery model implementation in Simulink with different sub-models and flow of information.

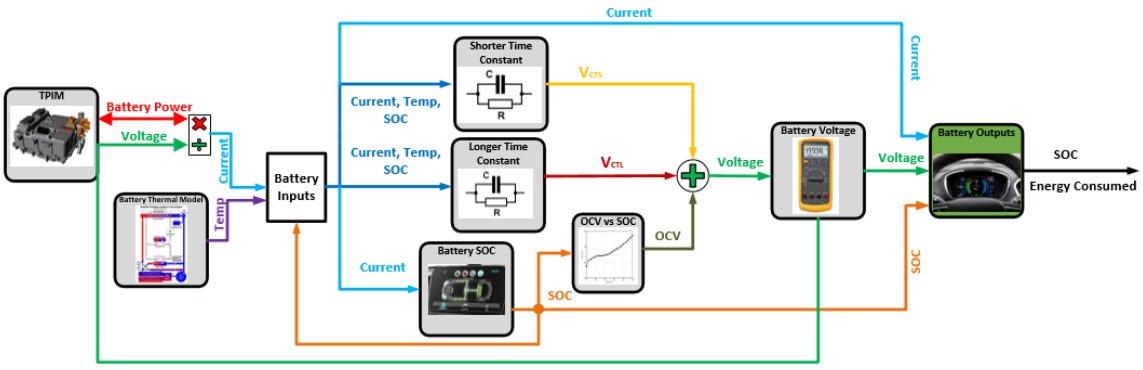

Figure 9. Battery Model Implementation

2.2.2. Battery Model Validation – SOC:

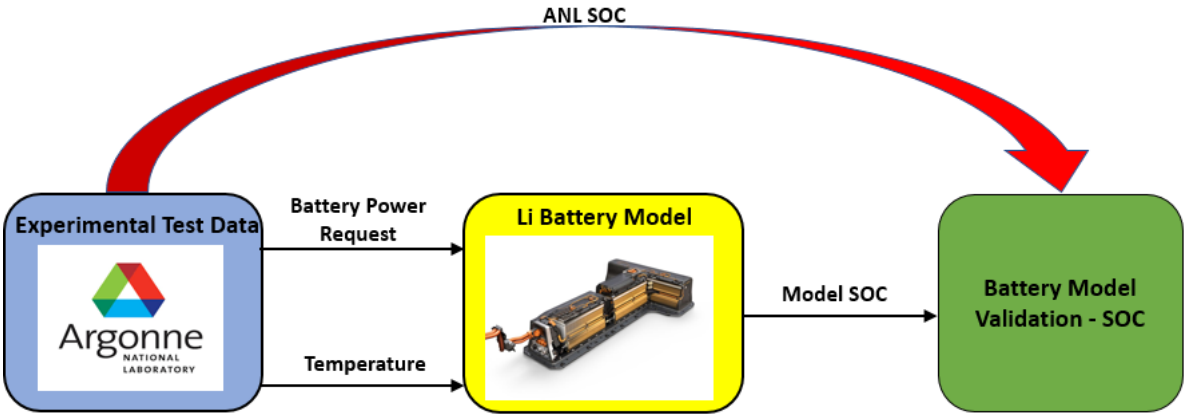

Figure 10. Battery SOC Validation Overview

The battery power request and temperature are given as inputs to the equivalent circuit dynamic model for different drive cycle in Charge Depleting Cases. The model is validated by comparing its SOC with the experimental SOC data from ANL. Figures 8-10 compares the model and ANL SOC results which shows very good correlation.

HWFET CD

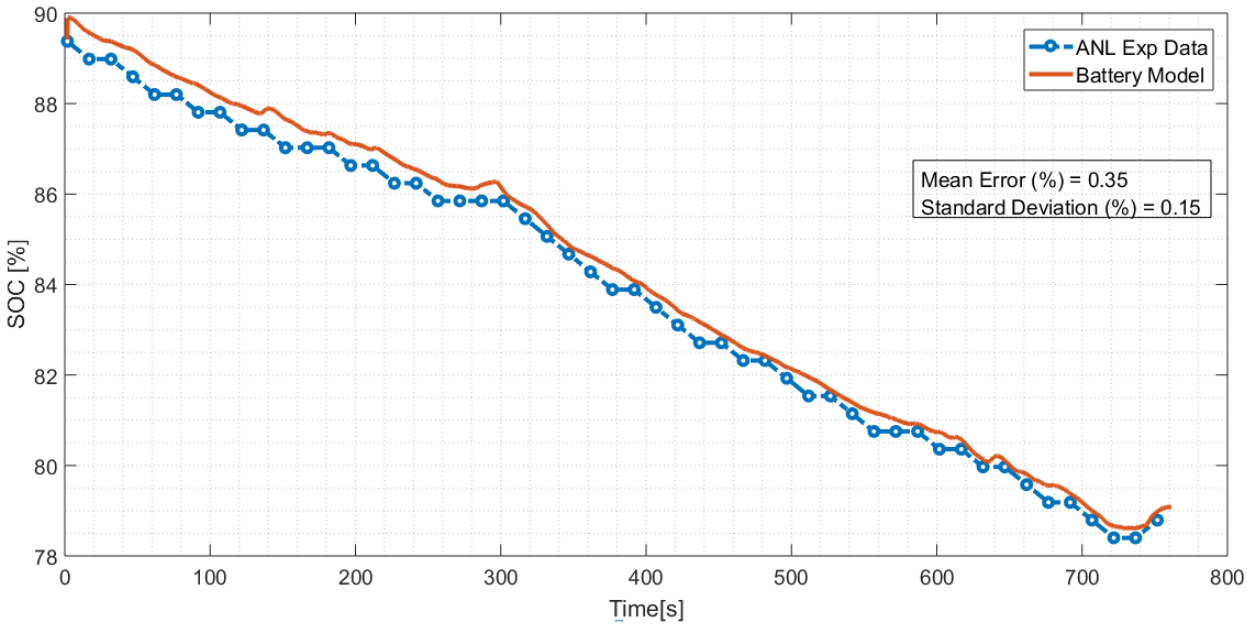

Figure 11. Battery Model Validation- HWFET CD (61707018.mat). Details in Appendix A1

UDDS Cycle CD

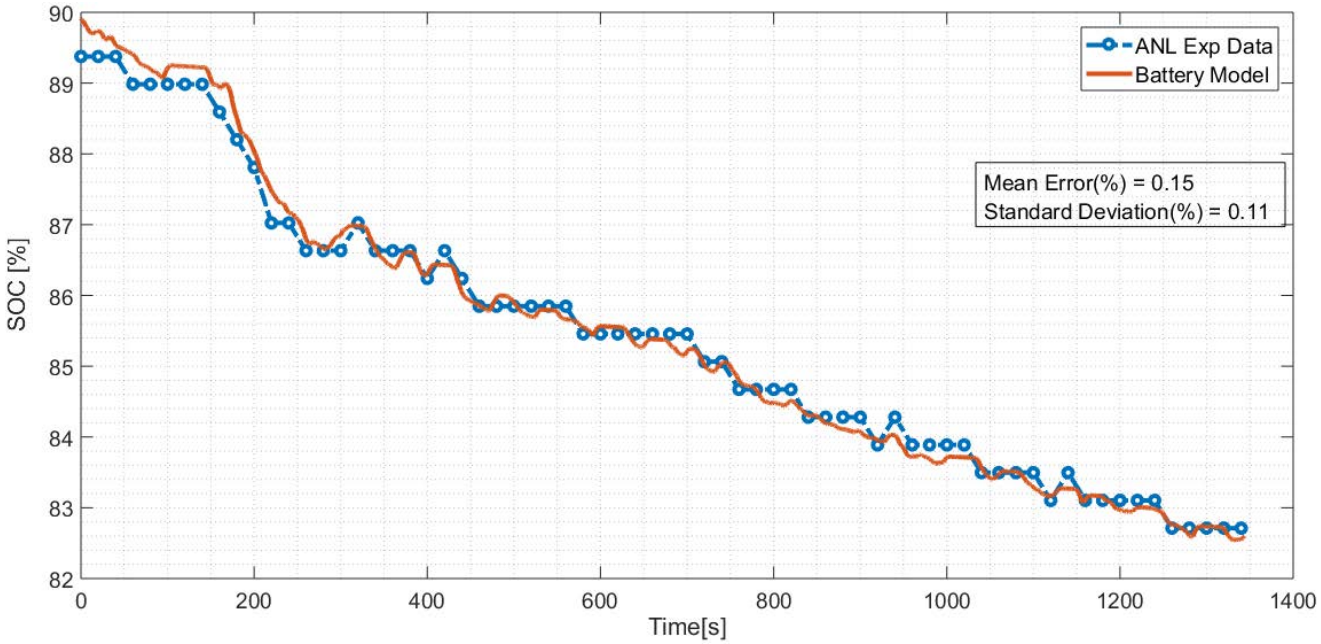

Figure 12. . Battery Model Validation- UDDS CD (61707020.mat). Details in Appendix A1

US06 Cycle CD

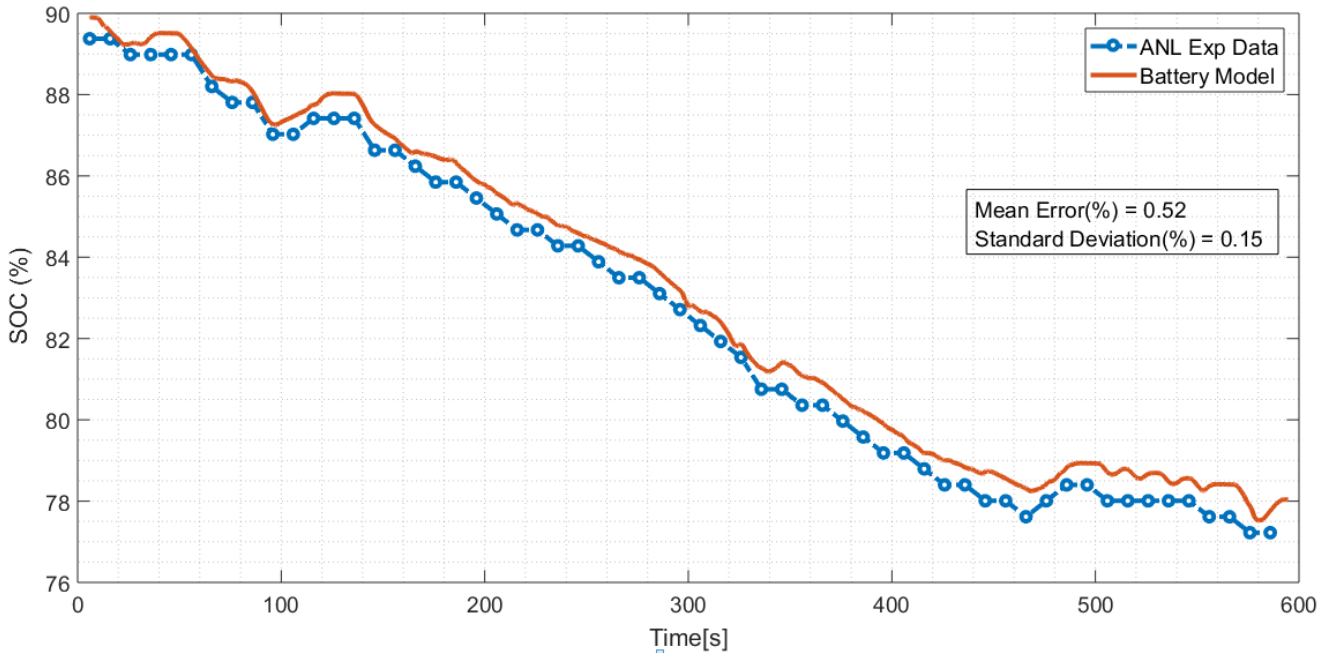

Figure 13.Battery Model Validation- US06 CD (61607019.mat). Details in Appendix A1

Table 2 summarizes the SOC validation for three drive cycles in CD mode and the mean error and standard deviation has been computed

Table 2. Battery Validation SOC

Test ID	Drive Cycle	Mean Error(%)	Standard Deviation (%)	Max Error(%)
61607018	HWFET CD	0.35	0.15	0.74
61607020	UDDS CD	0.15	0.11	0.52
61607019	US 06 CD	0.52	0.15	0.89

$$Mean\ Error\ (\%) = \frac{\sum_i^n (SOC_{model} - SOC_{exp})}{n} \quad (6)$$

2.2.3. Battery Thermal Model:

The battery heats up due to the Ohmic heating caused by the flow of current against an internal resistance. Battery heating due to irreversible exergy changes caused by chemical reactions is negligible in comparison to the ohmic heat generation and hence ignored. The battery current, open circuit and terminal voltages are used to determine the battery heating. Based on experimental data analysis it was observed that the battery's active liquid cooling system starts its cooling action when the battery temperature reaches above 33C.

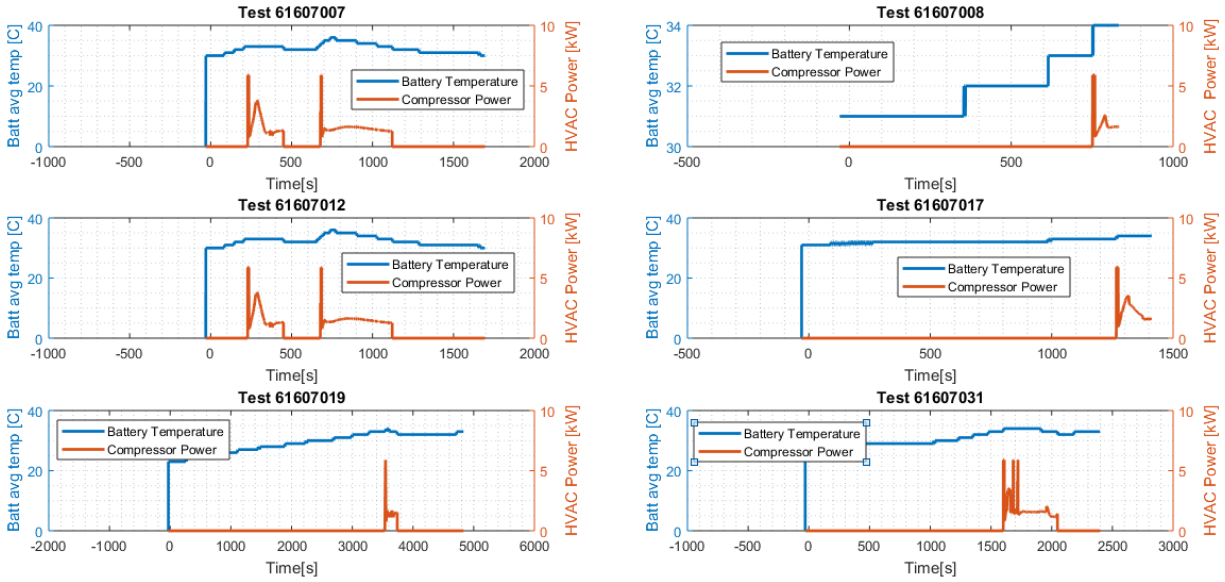

Figure 14. HVAC Compressor action due to battery cooling

Figure 14 shows the test cases where the HVAC compressor worked to cool the battery. The cutoff temperature for HVAC compressor action was found to be 33C which can be clearly seen in the case of test case 61607008 which is plotted below

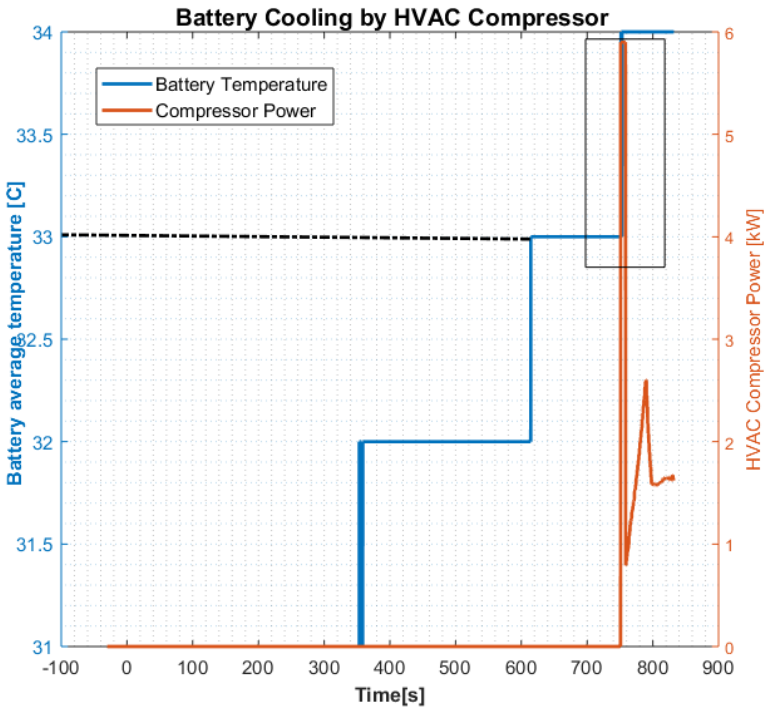

Figure 15. Battery Cooling Cutoff temperature 61607008

Battery cooling system works by circulating the liquid refrigerant through the battery pack. The liquid refrigerant at lower temperature absorbs the heat from the battery cell through convective heat transfer.

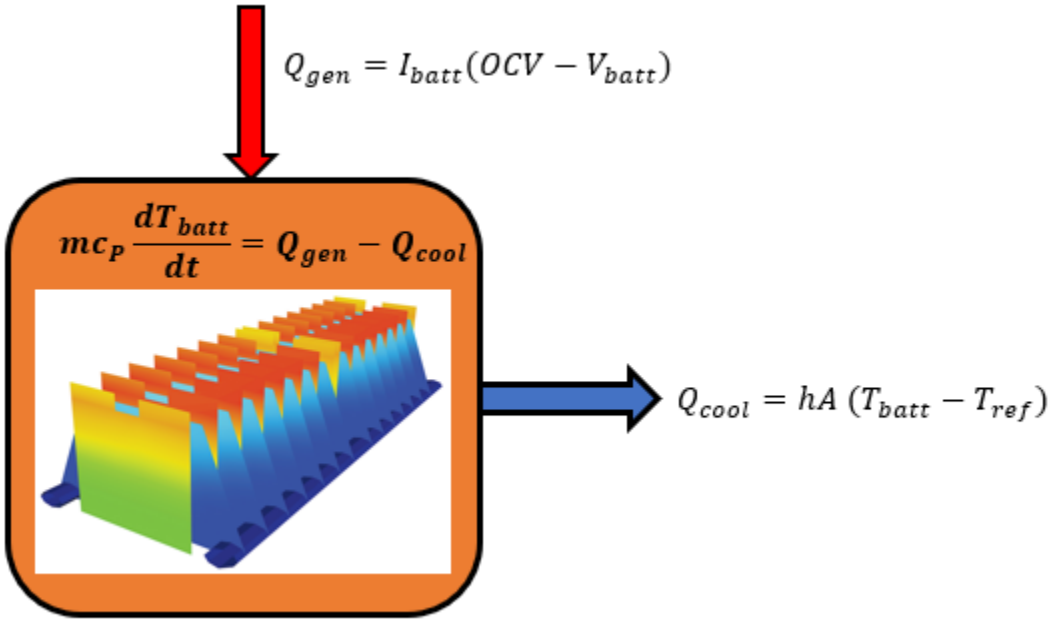

Figure 16. Battery Thermal Model

To predict the cooling system action correctly we need to track the battery temperature. A lumped thermal model is used to calculate the battery temperature based on the assumption that the temperature is uniform inside the battery pack. Figure 14 shows the battery cooling model. The ohmic heat generation Q_{gen} is the heat input to the system and Q_{cool} is the heat out from the system due to liquid cooling. Based on the energy balance equation:

$$mC_P \frac{dT_{batt}}{dt} = Q_{gen} - Q_{cool}$$

$$mC_P \frac{dT_{batt}}{dt} = I_{batt}(OCV - V_{batt}) - hA\,(T_{batt} - T_{ref})$$

Where m is the mass of the battery pack (183kg), C_P is the specific heat capacity of battery, T_{batt} is the lumped battery temperature

I_{batt} , V_{batt} and OCV are the battery currents, terminal and open circuit voltages respectively

h is the convective heat transfer coefficient , A is the area available for heat transfer and T_{ref} is the refrigerant temperature.

Note the convective heat transfer coefficient is typically affected by the mass flow rate of refrigerant and geometry and thermal conductivity of the heat transfer interfaces. Among those parameters only refrigerant mass flow rate is the variable. Hence the heat transfer coefficient is affected mainly by mass flow rate which in turn depends on the battery temperature and amount of heat generated

$$h = fn(\dot{m}_{ref}) = fn\,(T_{batt}, Q_{gen})$$

To perform continuous battery cooling action and refrigerant complete its thermodynamic cycle the refrigerant has to reject the heat absorbed from the battery to the environment The heat rejection is accomplished through the HVAC compressor operation and a heat exchanger. To compress the hot refrigerant the HVAC compressor draws significant electrical energy from the battery and thus it becomes important to include the energy consumed by the HVAC compressor in the total energy calculation. An empirical relation is proposed to estimate the total energy consumed by the compressor

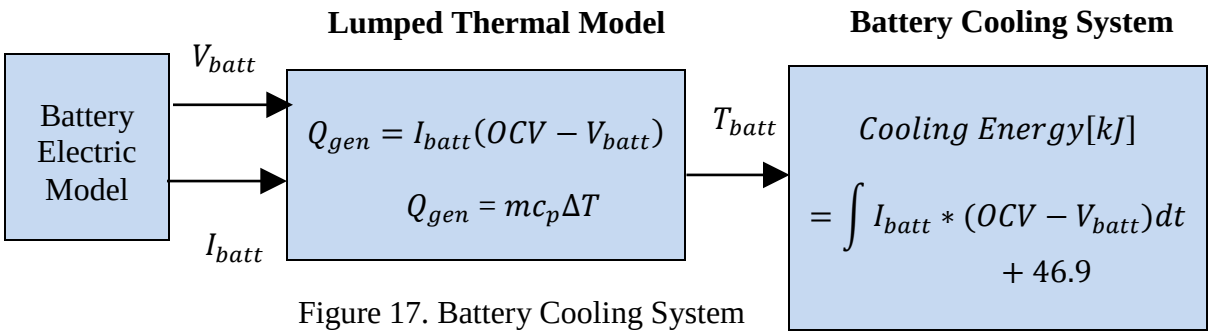

Figure 17. Battery Cooling System Model

Due to lack of extensive test data to characterize HVAC compressor action it was assumed that the HVAC compressor energy was equal to cooling load on the battery i.e. the battery heat energy gained after the cut off temperature of the cooling systems. Figure 15 summarizes the approach.

$$Cooling\ Energy[kJ] = \int I_{batt} * (OCV - V_{batt})dt + 46.9$$

The 45.8 KJ was observed to be the initial energy required to start the compressor. The battery cooling system is activated when the battery temperature reaches above 33C. This is calculated by integrating the initial step HVAC compressor power for the six test cases. and averaging them.

Table 3. Compressor Starting Energy

Drive Cycle ID	HVAC Compressor Energy Simulation [KJ]
61607007	47.8
61607008	43.7
61607012	44.8
61607017	46
61607019	51.3
61607031	47.8

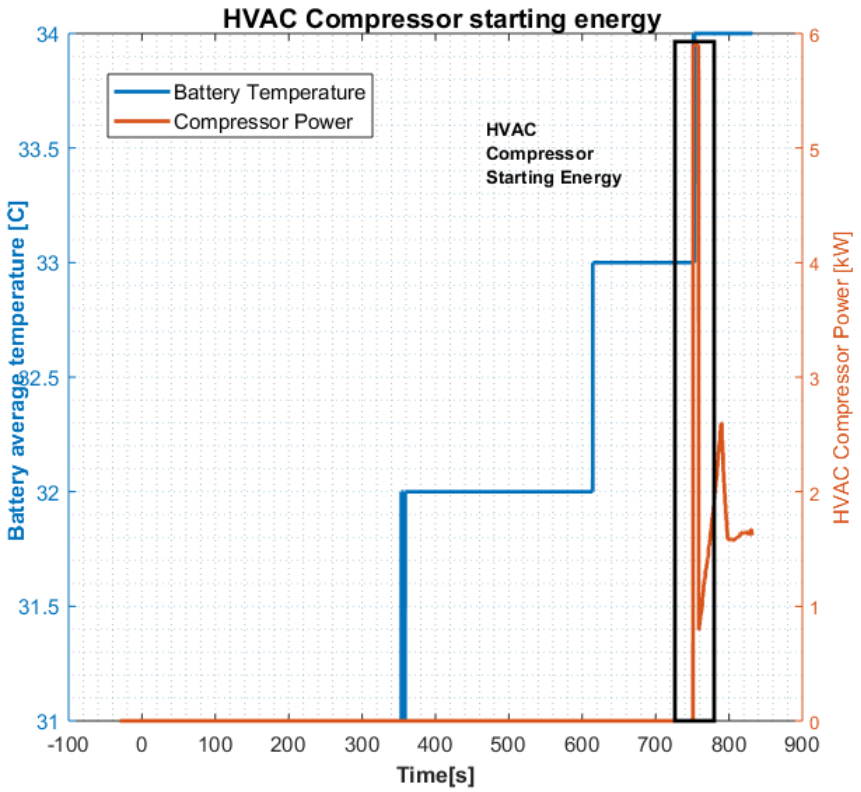

Figure 18. HVAC Compressor Starting Energy

The cooling energy or load is taken as the equivalent amount of battery thermal energy stored above 33C i.e. the battery cooling system integrates the battery ohmic heating for temperatures above 33C. It was also observed that the battery cooling system stopped working when the temperature dropped to 32C which indicates a hysteresis of 1℃ which is consistent with the rules implemented [24]

Two of the drive cycles shows good results when using this lumped empirical approach. For the other five drive cycles where HVAC compressor worked for battery cooling, the data acquisition stopped in the process of battery cooling and experimental data is insufficient for validation.

Table 4. Battery Cooling system Empirical Model

Drive Cycle ID	HVAC Compressor Energy Simulation [KJ]	HVAC Compressor Energy Experimental [KJ]	Relative Error
61607012	1047.9	1096.5	4.4
61607019	321.6	310.5	3.6

2.3. Electric Motor and TPIM Inverter Model

Chevy Volt uses 2 motor generators namely Motor Generator A and Motor Generator B for propulsion and regenerative braking. The power required by the motors to drive the vehicle has been obtained from performance maps provided by GM. The tests have been performed in an integrated manner to characterize the combined performance of the motor and inverter module. Figure 13 and 14 shows the contour maps of motor efficiency as a function of Torque and Speeds.

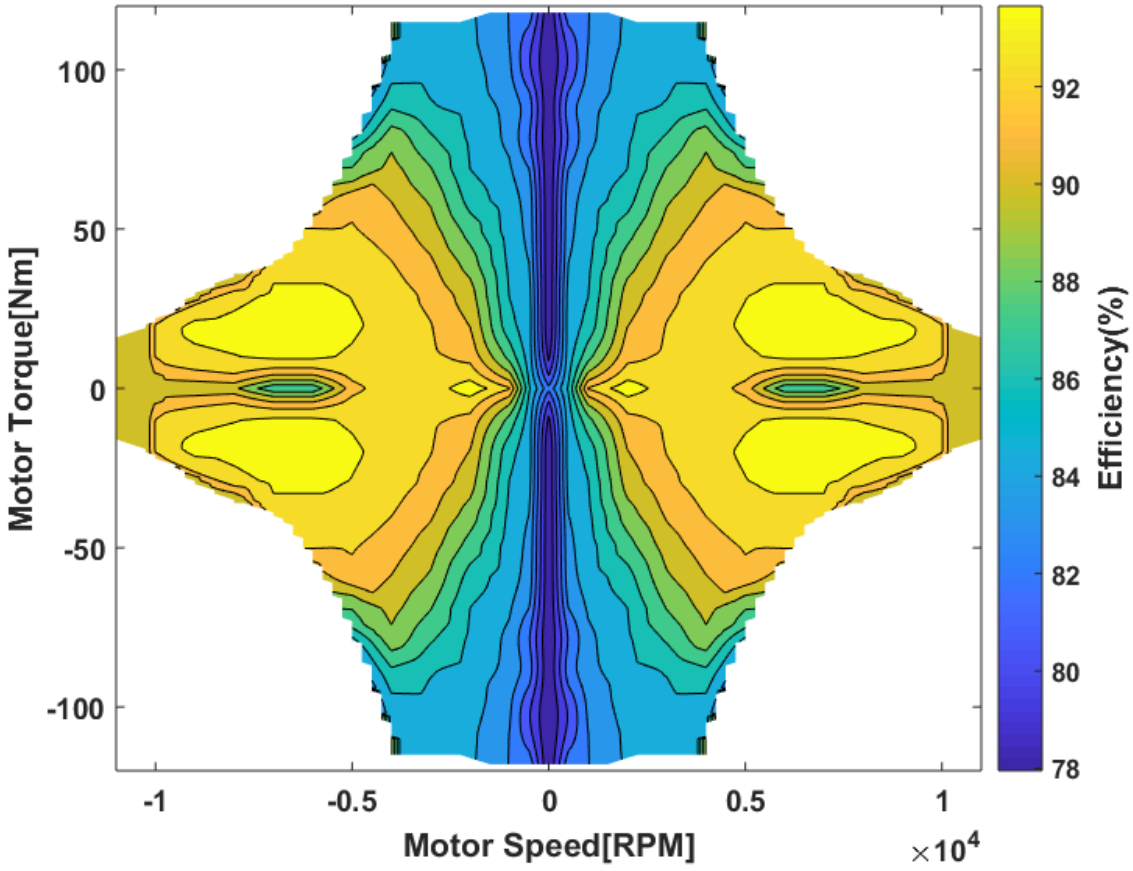

Figure 19. Motor A Efficiency Map

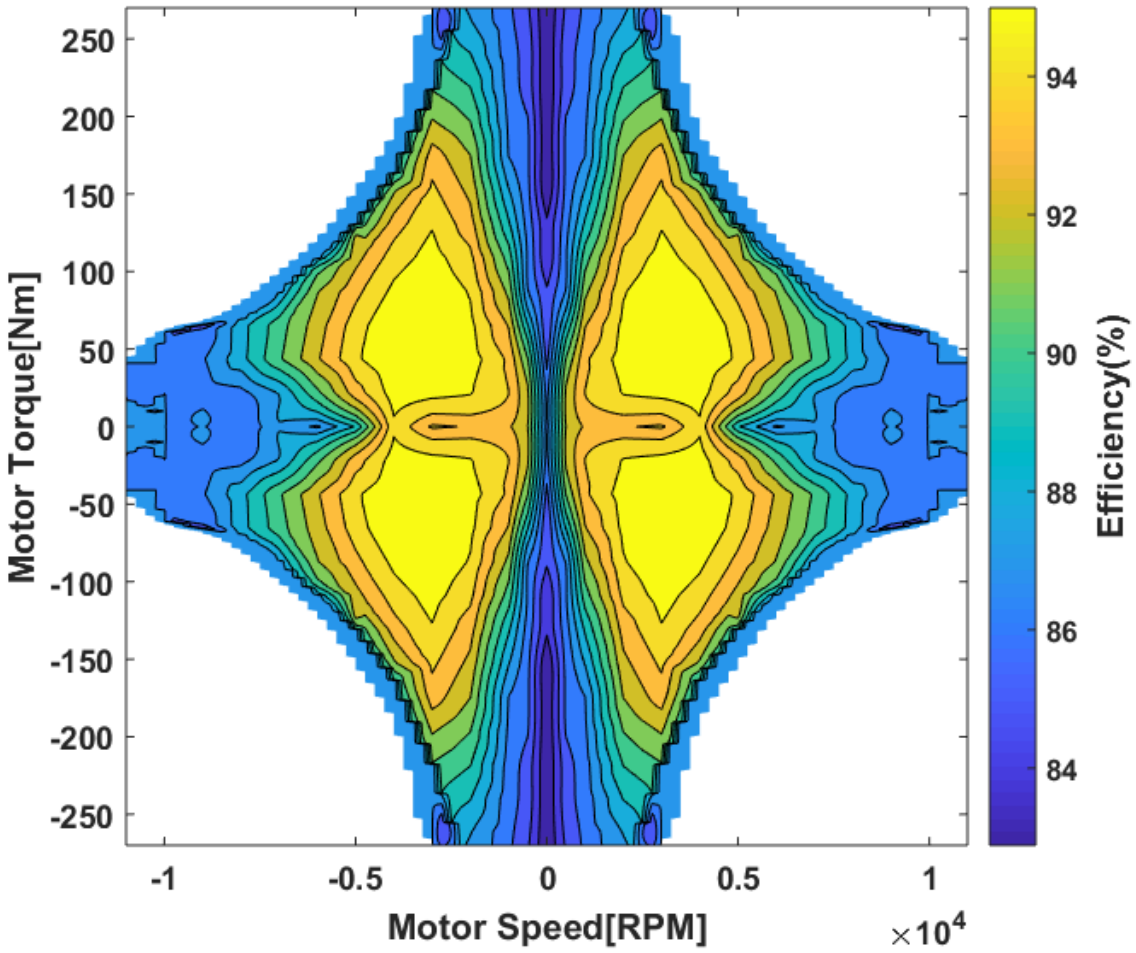

Figure 20. Motor B Efficiency Map

The efficiency of the motor and TPIM inverter is always the ratio of output and input energy. Since the power flow direction is different in both traction and regeneration cases the efficiency is calculated differently depending on power flow.

During traction, the electrical power from motor is converted to mechanical power in the drive unit which is sent to the wheels. Therefore

$$Motor\ Efficiency(\%) = \frac{Mechanical\ Power}{Electrcial\ Power} = \frac{Motor\ Torque * Motor\ Speed}{Electrical\ Power} \quad (7)$$

During regeneration, the mechanical power from the drive unit is converted to electrical power causing the motor to spin in the reverse direction.

During regeneration, the motor efficiency is defined as following

$$Motor\ Efficiency(\%)\frac{Electrical\ Power}{Mechanical\ Power} = \frac{Electrical\ Power}{Regen\ Torque * Motor\ Speed} \quad (8)$$

Figure 15 and 16 similarly shows the contour maps of TPIM inverter efficiency for Motor A and B as function of corresponding Motor Torques and Speeds.

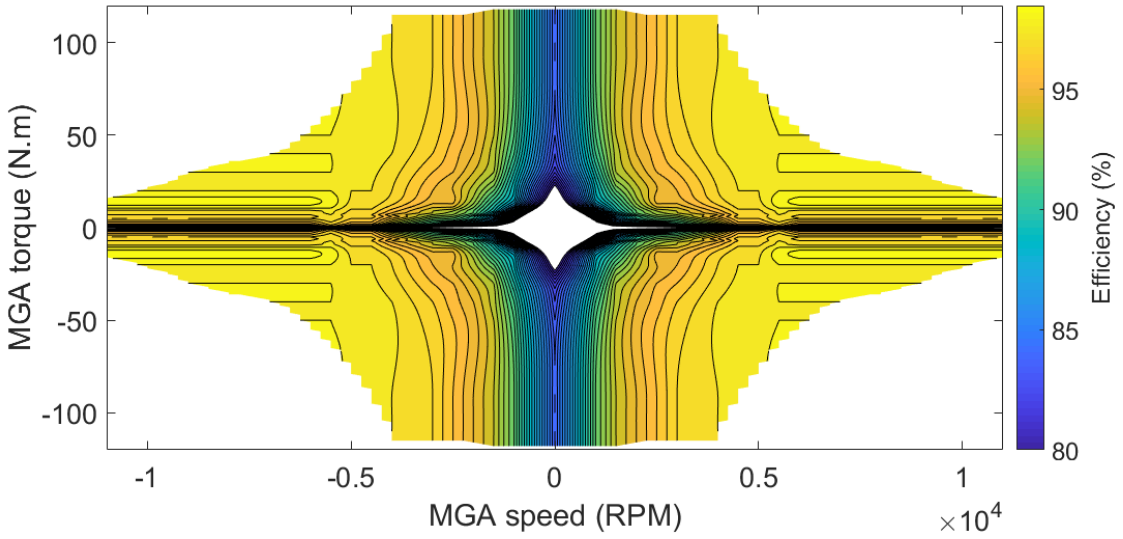

Figure 21. TPIM Inverter A Efficiency

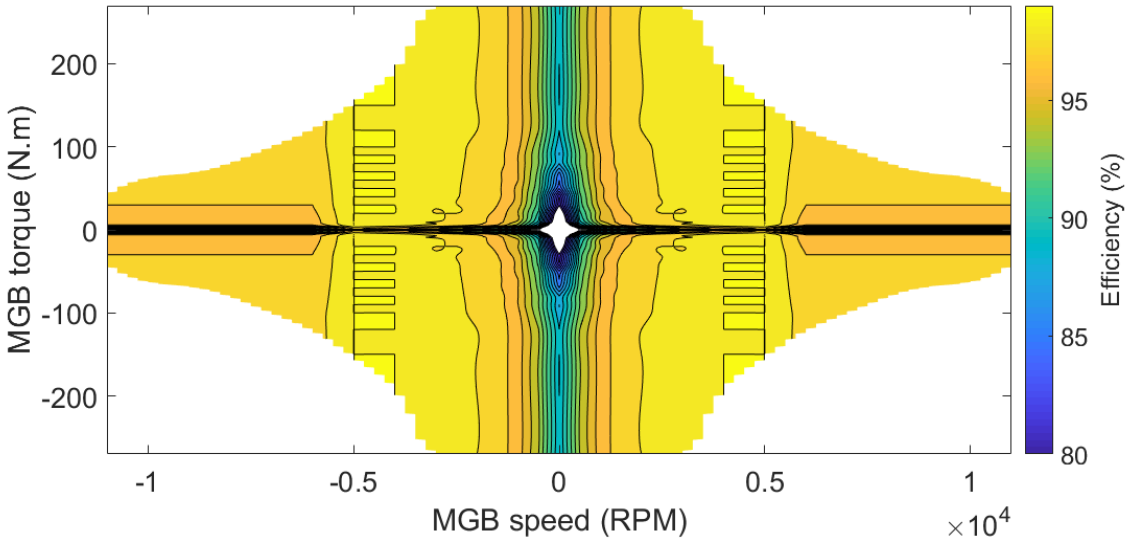

Figure 22. TPIM Inverter B Efficiency

The TPIM inverter forms the interface between the battery and motor modules which

i. Battery DC power to motor AC power during traction
ii. Motor AC power to Battery DC power during regeneration

During traction, TPIM efficiency is as follows

$$TPIM\ Efficiency(\%) = \frac{Motor\ Electrical\ Power}{Battery\ Power} = \frac{Motor\ Electrical\ Power}{Battery\ Voltage * Current} \quad (9)$$

During regeneration, TPIM efficiency is as follows

$$TPIM\ Efficiency(\%) = \frac{Battery\ Power}{Motor\ Electrical\ Power} = \frac{Battery\ Voltage * Current}{Motor\ Electrical\ Power} \quad (10)$$

2.3.1. Motor and TPIM Inverter Validation

Based on the ANL experimental inputs data of Motor Speeds, Torque and operating voltage we test the accuracy of the motor and inverter performance maps by comparing the battery power request from the model with the ANL battery power request values. Figure 17 shows the overall schematic of the motor model validation

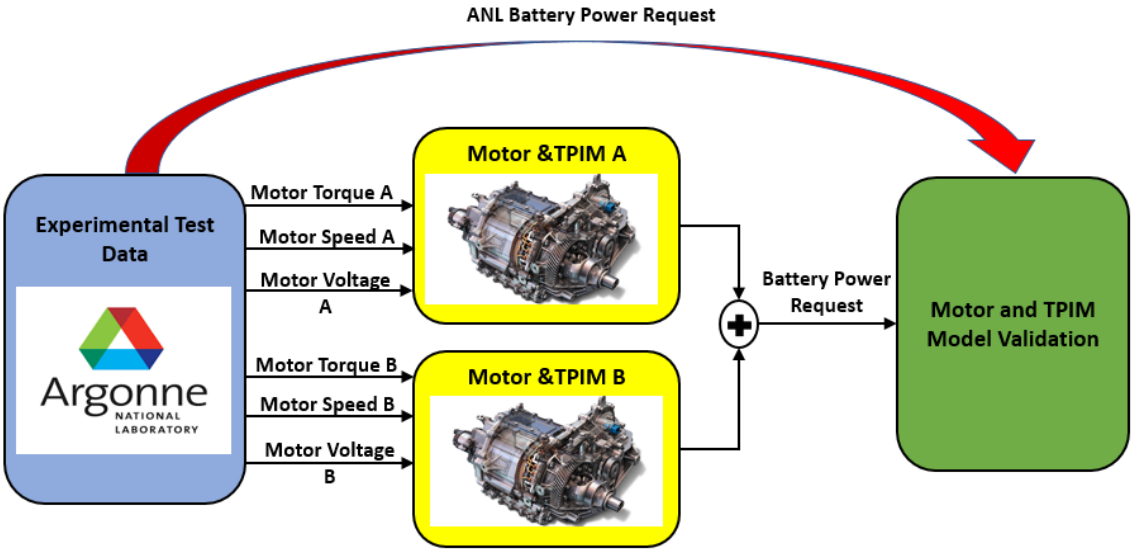

Figure 23. Motor Model Validation Schematic

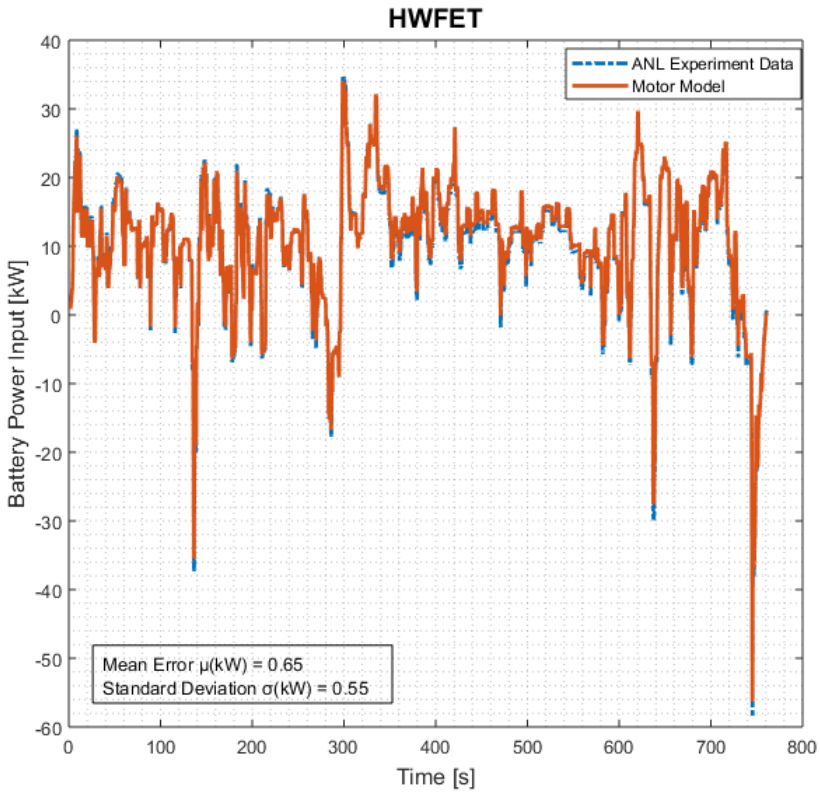

Figure 24. Motor Model Validation- HWFET CD (61607018.mat). Details in Appendix A2

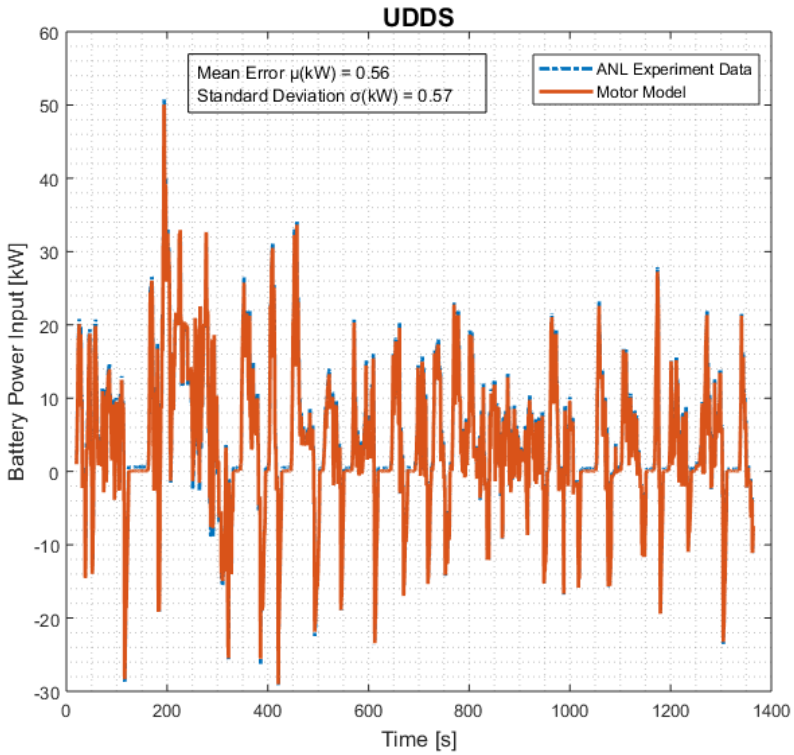

Figure 25.Motor Model Validation- UDDS CD (61607020.mat). Details in Appendix A2

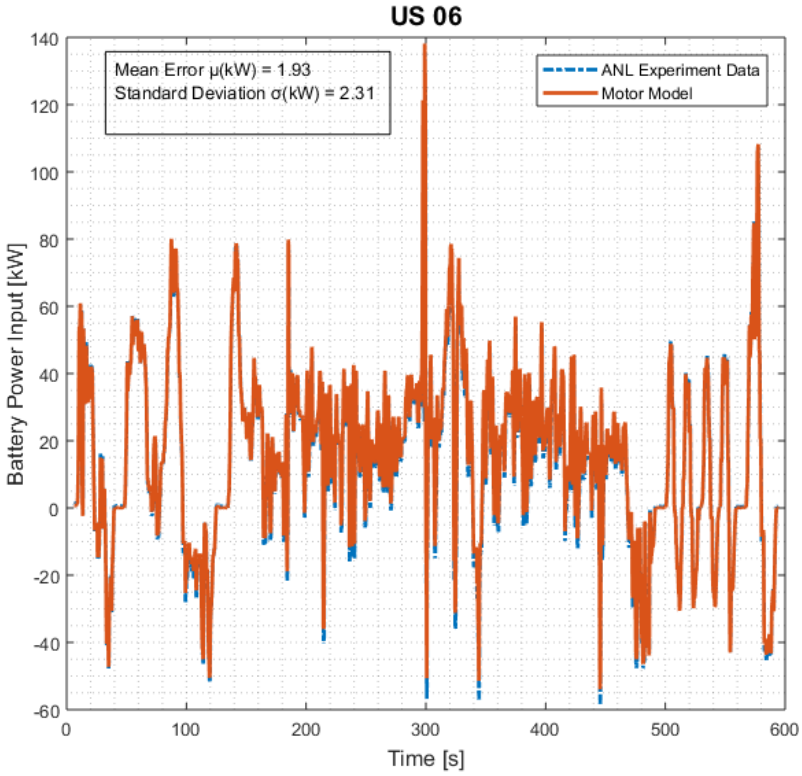

Figure 26. Motor Model Validation- US06 CD (61607019.mat). Details in Appendix A2.

2.4. Drive Unit Model:

As stated before Chevy Volt has two operating modes in EV namely 1-Motor EV mode where motor generator B provides the traction/regen requirements and 2-Motor EV mode where motor generator A assists B in traction demand.

2.4.1. One Motor EV Mode:

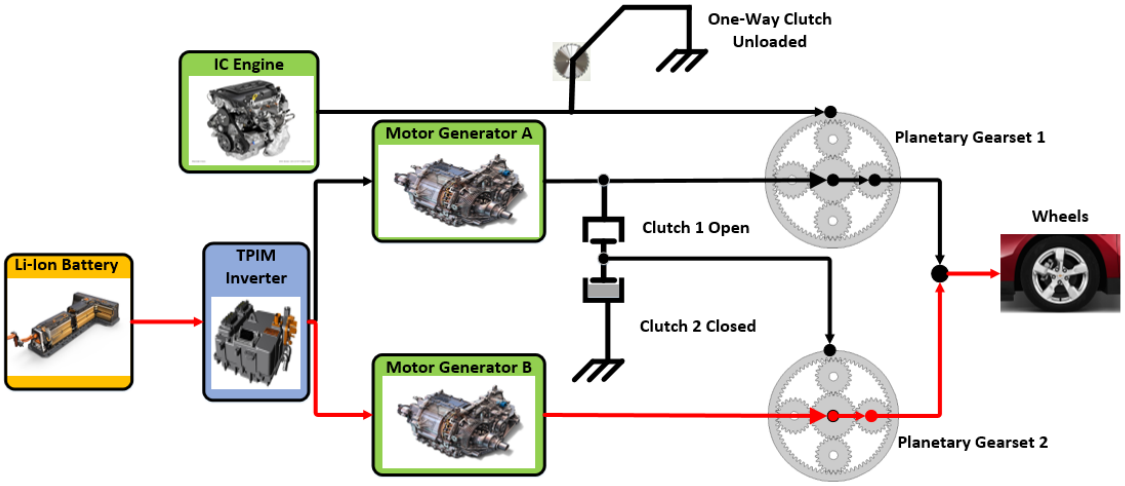

Figure 27. EV Mode1 Power Flow

Mode 1 is used for light load operational requirements. The Clutch C1 is open and clutch C2 is closed. The One Way Clutch (OWC) in unloaded since the planetary gear set does not receive any power from motor generator A.

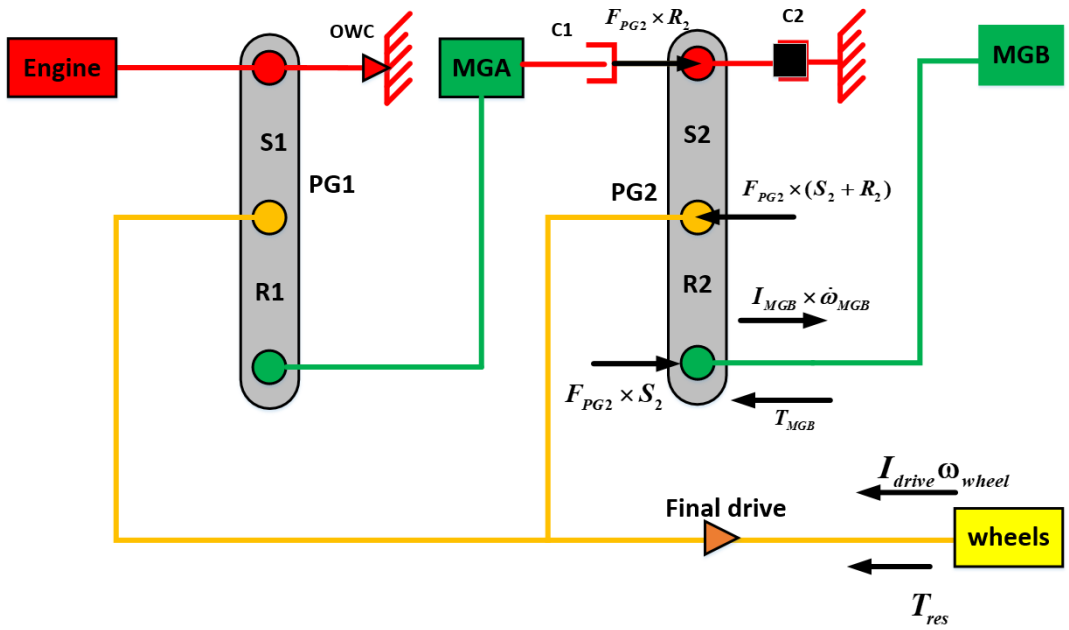

Figure 28. EV Mode 1 Lever Diagram

Based on the force balance in the above lever diagram we obtain the following dynamic equations[22]:

$$\begin{bmatrix} I_{drive} & 0 & 0 & S_1 + R_1 & S_2 + R_2 \\ 0 & I_{MGA} & 0 & -S_1 & 0 \\ 0 & 0 & I_{MGB} & 0 & -S_2 \\ S_1 + R_1 & -S_1 & 0 & 0 & 0 \\ S_2 + R_2 & 0 & -S_2 & 0 & 0 \end{bmatrix} \begin{bmatrix} \dot{\omega}_{wheel} \\ \dot{\omega}_{MGA} \\ \dot{\omega}_{MGB} \\ F_{PG1} \\ F_{PG2} \end{bmatrix} = \begin{bmatrix} -T_{res} \\ 0 \\ T_{MGB} \\ 0 \\ 0 \end{bmatrix} \quad (11)$$

Where I_{drive} and I_{MGB} are the inertias of the driveline and propulsion component Motor Generator B. T_{res} is the sum of torque caused by vehicle resisitance and T_{MGB} is the torque supplied by MGB. S_2 and R_2 are the radii of sun and ring gear for planetary gear 2. F_{PG2} is the internal force acting on planetary gear 2 by planetary gear 1. $\dot{\omega}_{wheel}$ and $\dot{\omega}_{MGB}$ are the angular acceleration of the wheels and motor generator B.

2.4.2. Two Motor EV Mode:

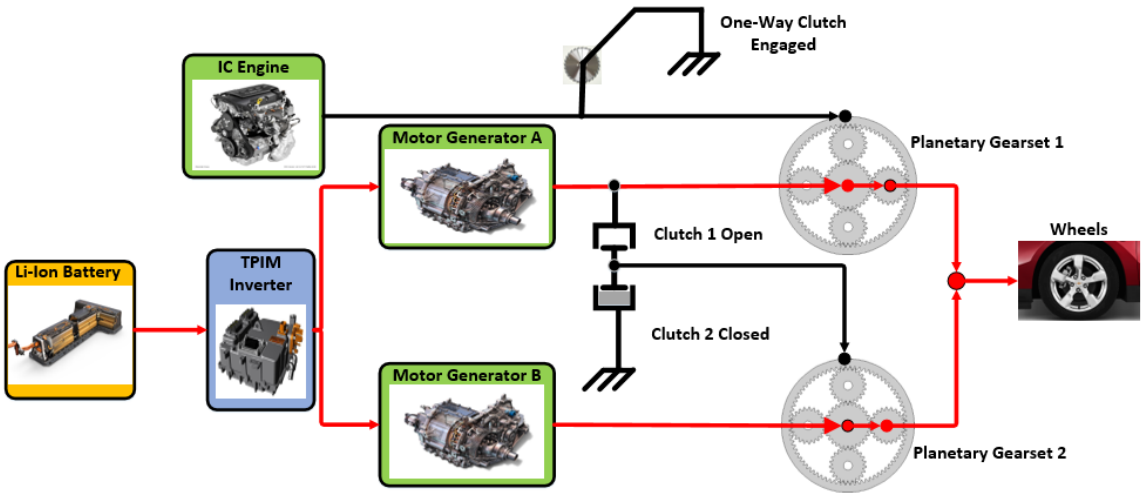

Figure 29. EV Mode 2 Power Flow

Mode 2 i.e. two motor EV mode is used when Motor Generator B cannot handle high loads and for smooth acceleration in vehicle starts. Similar to mode 1 Clutch C1 is open and clutch C2 is closed. However the One Way Clutch (OWC) is engaged to prevent the engine from turning due to rotation of planetary gear 2 by Motor generator A.

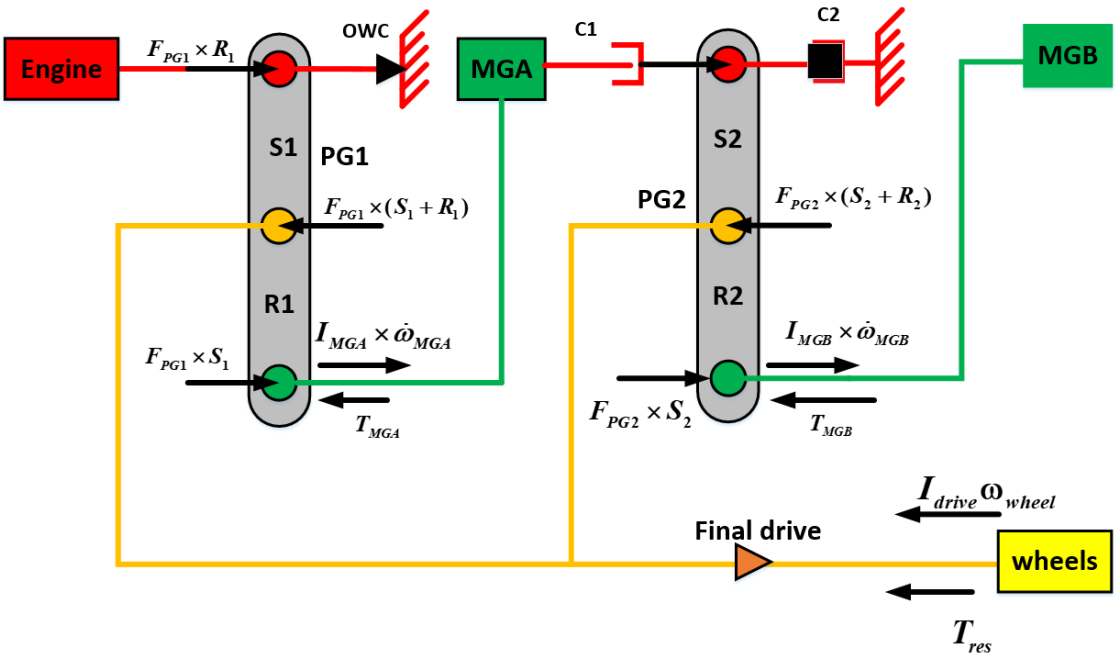

Figure 30. EV Mode 2 Lever Diagram

Based on the lever diagram we obtain the following dynamic equations[22]

$$\begin{bmatrix} I_{drive} & 0 & 0 & S_1 + R_1 & S_2 + R_2 \\ 0 & I_{MGA} & 0 & -S_1 & 0 \\ 0 & 0 & I_{MGB} & 0 & -S_2 \\ S_1 + R_1 & -S_1 & 0 & 0 & 0 \\ S_2 + R_2 & 0 & -S_2 & 0 & 0 \end{bmatrix} \begin{bmatrix} \dot{\omega}_{wheel} \\ \dot{\omega}_{MGA} \\ \dot{\omega}_{MGB} \\ F_{PG1} \\ F_{PG2} \end{bmatrix} = \begin{bmatrix} -T_{res} \\ T_{MGA} \\ T_{MGB} \\ 0 \\ 0 \end{bmatrix} \quad (12)$$

Where I_{drive}, I_{MGA} and I_{MGB} are the inertias of the driveline and propulsion components Motor Generator A and B. T_{res} is the sum of torque caused by vehicle resisitance and T_{MGA}, T_{MGB} are the torques supplied by MGA and MGB respectively. S_1, S_2 and R_1 R_2 are the radii of sun and ring gear of planetary gears 1 and 2 respectively. F_{PG2} is the internal force acting on planetary gear 2 by planetary gear 1.Similarly F_{PG1} is the internal force acting on planetary gear 1 by planetary gear 2. $\dot{\omega}_{wheel}$ $\dot{\omega}_{MGA}$ and $\dot{\omega}_{MGB}$ are the angular acceleration of the wheels, motor generators A and motor generators B respectively.

2.5. Vehicle Dynamics Model:

The Longitudinal vehicle dynamics relations for Chevy Volt has been discussed in this section.

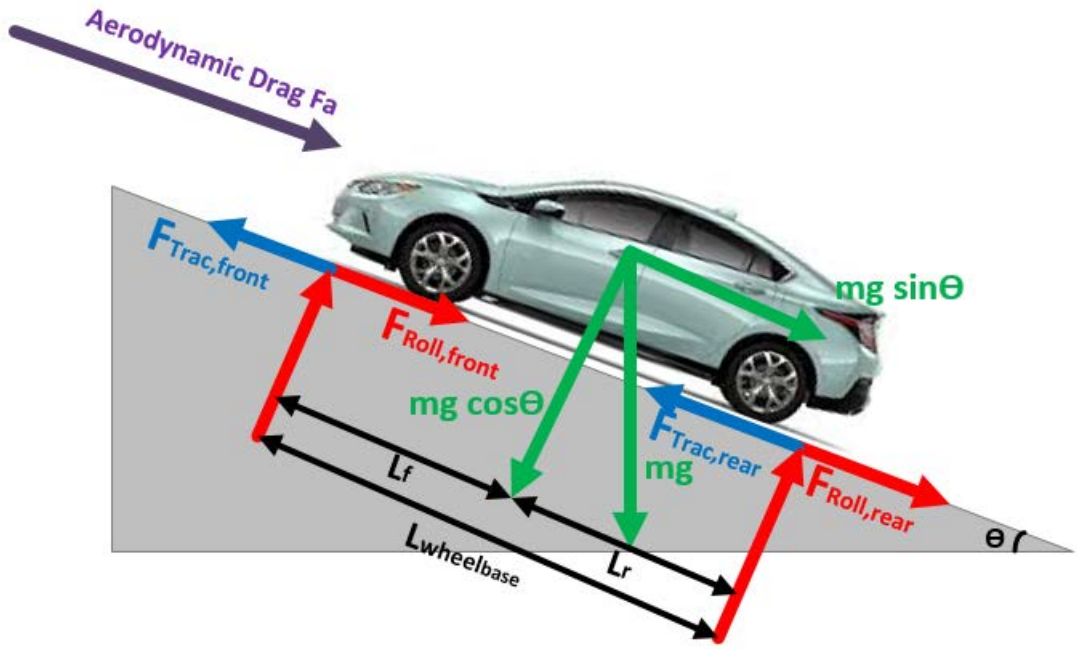

Figure 31. Longitudinal Vehicle Dynamics

From Newton's Second Law we obtain the vehicle acceleration as follows

$$ma = F_T - F_R \tag{13}$$

Where F_T is the sum of tractive forces at the front wheels (front wheel drive), F_R is the sum of the resistive forces, m is the mass of the vehicle and a is the acceleration of the vehicle.

The resistive forces include the rolling resistance, aerodynamic drag and gradient resistance forces

$$F_R = F_{roll} + F_{grade} + F_{aero} \tag{14}$$

Alternatively, the resistive forces are found by the road load equation as follows

Road load equation:

$$F_R = F_o + F_1 v + F_2 v^2 \quad (15)$$

The coefficients F_o, F_1 and F_2 are known as road load coefficients and have been provided by ANL. The road load force is exerted on the vehicle when driving on a smooth level surface such as tire rolling resistance, aerodynamic drag and driveline losses and therefore it ignores the grade resistance. Since all our validation cases consist of only zero grade surfaces (level roads) the road load equation accurately represents the total resistance forces on the vehicle.

Table 5. ANL Road Load Coefficients

Coefficient	**Value**
F_o (N)	143.46
F_1 (N/Kph)	1.1461
F_2 (N/kph^2)	0.01185

2.6. Transmission Auxiliary Pump and Spin Losses:

The transmission auxiliary pump circulates the transmission fluid which is used to lubricate the moving parts of the automatic transmission. In addition to lubrication it serves to remove the heat generated within the transmission. Performance maps characterizing the auxiliary pump and inverter efficiency based on auxiliary pump speed and torque has been implemented into the model.

$$Aux\ Pump\ Power = \frac{Aux\ Pump\ Torque(Nm) * Aux\ Pump\ Speed(RPM) * \pi}{\eta_{pump} * \eta_{inv} * 30} \quad (16)$$

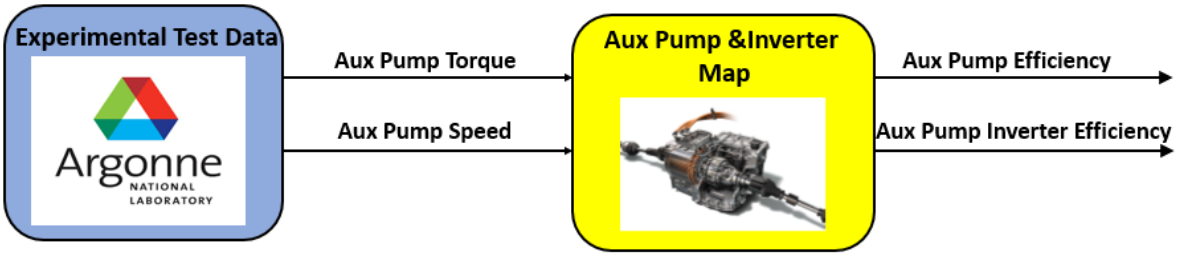

Figure 32. Auxiliary Pump Model

Transmission spin losses are due to the drag created by lubricating oil on the gear and open clutch faces. It is also caused by the churning of oil, viscous dissipation of bearing and squeezing of oil in the gear mesh cavities. Look up tables characterizing the spin loss based on the transmission input speed, output speed, line pressure and oil temperature have been provided by GM and has been implemented in the model. The transmission spin losses reduce the torque transferred to the wheels. To counter these losses the motors have to supply greater amount of torque and as a result, the energy consumption increases. The spin loss determines the motor torque which in turn affects the total energy consumption.

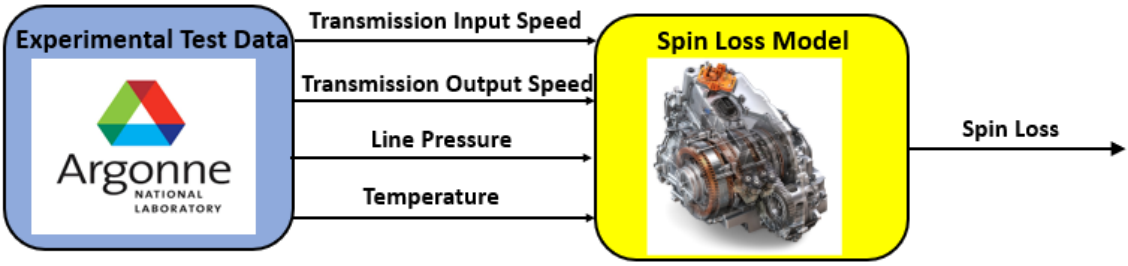

Figure 33. Transmission Spin Loss model

The transmission speed is the speed of the ring gear which in EV mode remains zero. The transmission output speed is the pre-final drive speed. The transmission line pressure was taken to be an average value of 600 KPa and temperature was considered to be 70℃ for all validation cases

2.7. EV Mode Selection and Torque Blending Logic:

Based on the data analysis of ANL experimental data the rules for EV mode selection and motor torque blending values were obtained

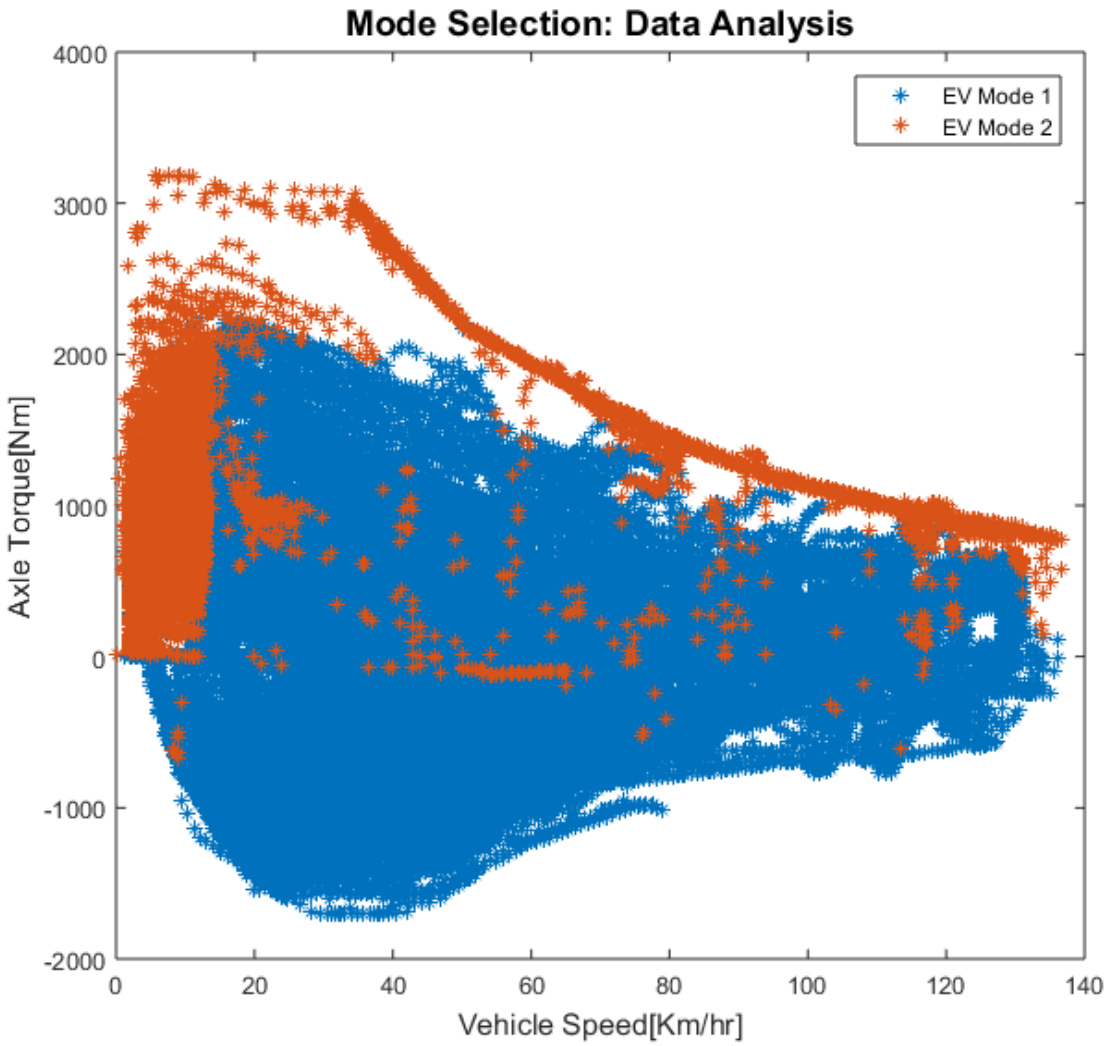

Figure 34. ANL Mode Selection Data Points

Figure 30 has been obtained by plotting of axle torque and vehicle speed data points from the ANL experimental data. This characterization of modes as a function of axle torque and vehicle speed is used in the EV supervisory controller to determine the modes based on the model inputs. Note that while determining the boundary the operations regions of the some of the ambiguous mode points where it is possible to have both modes in a certain region of axle torque and vehicle speed have been ignored by considering those points as hysteresis time for the mode switch.

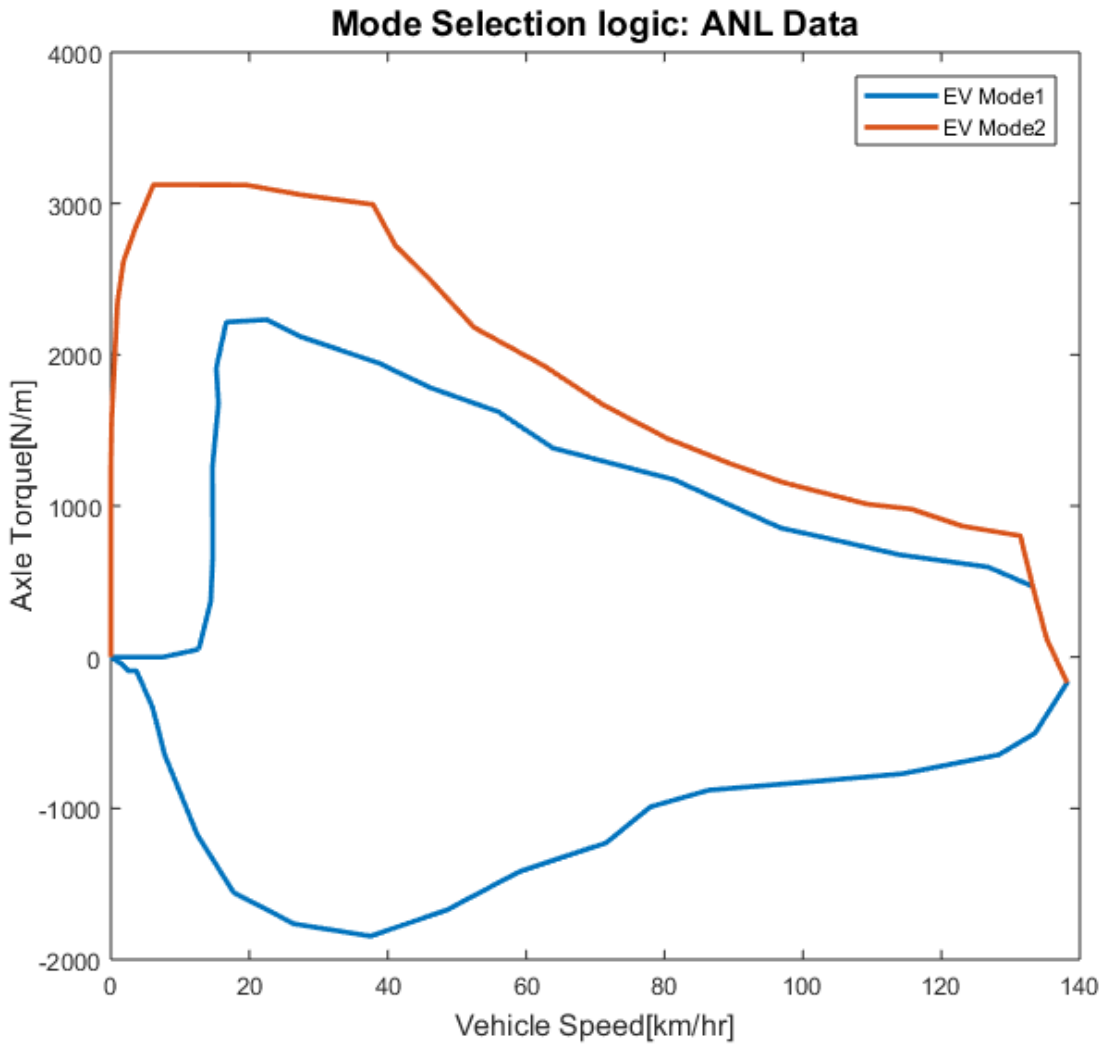

Figure 35.Mode Selection regions

Control Logic:

From figures 30 and 31, it can be seen for vehicle speeds less than 15 km/hr the vehicle operated in two motor EV mode. This is consistent with the control logic implemented in the vehicle for a smooth and swift launch from standstill where both motors provide the torque request[8]. The torque was split among the motors in the following ratio to maximize the efficiency of motor operation [23].

$$\frac{Motor\ A\ Torque}{Motor\ B\ Torque} = \frac{1}{9} \tag{17}$$

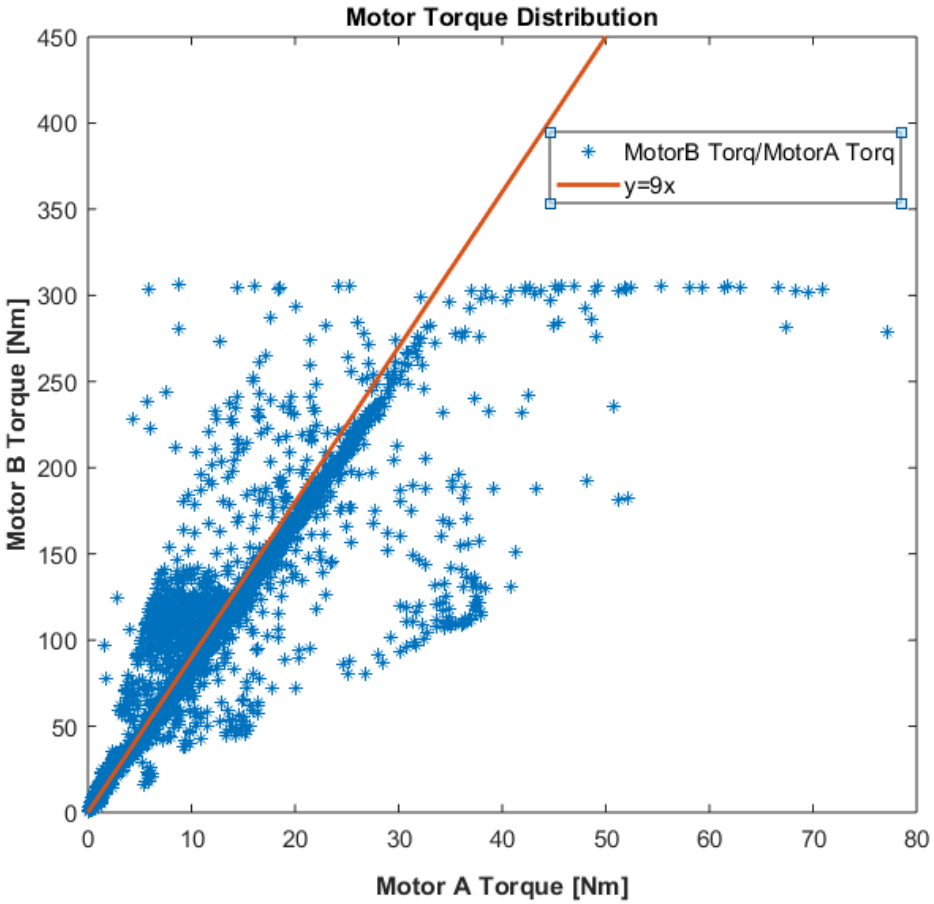

Figure 36. Torque blending between Motor A and Motor B

For vehicle speeds greater than 15 km/hr, the axle torque request was compared against the maximum axle torque possible by Motor B. If the axle torque request exceeds the Motor B maximum limit, the vehicle operates in 2 motor EV mode with Motor B providing its maximum torque capability and the rest supplemented by Motor A.

If axle torque request falls within the maximum values the vehicle operates in 1-Motor EV mode with motor B providing the entire axle torque request and motor A providing no power.

The control logic is summarized in the following flowchart:

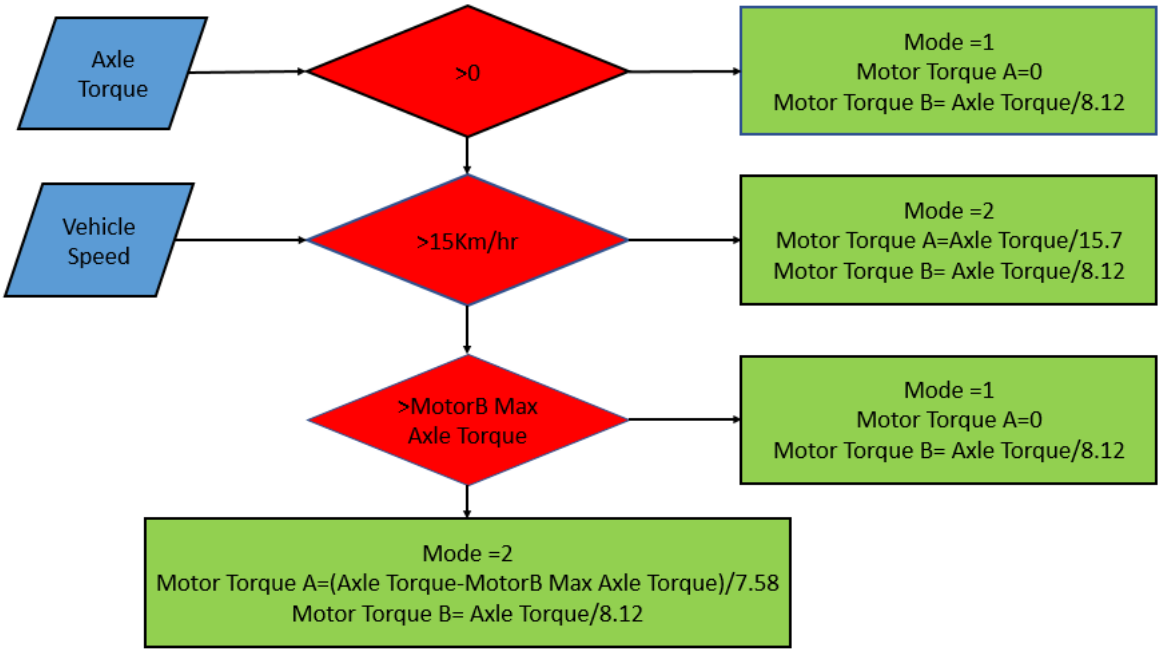

Figure 37. Mode Selection logic and torque blending ratio

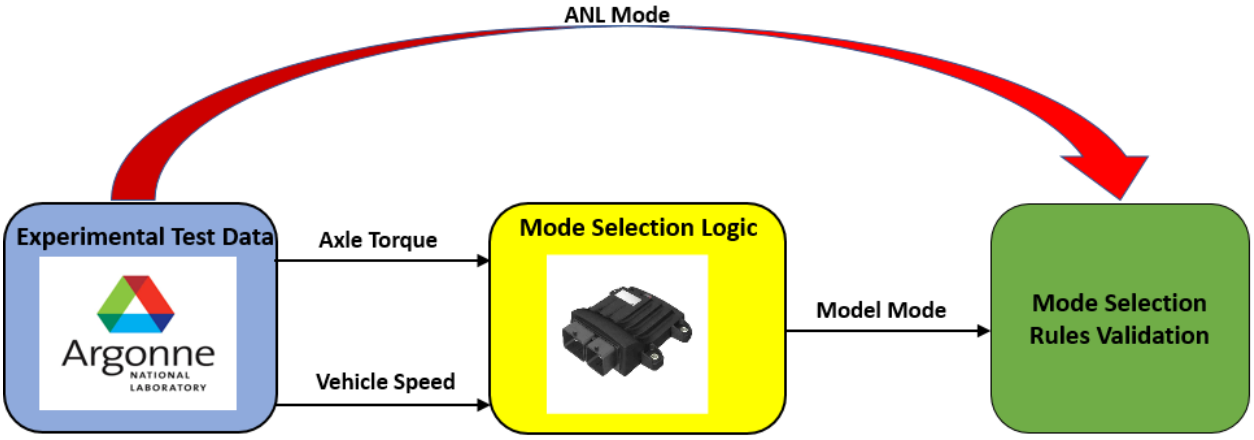

Figure 38. ANL Mode Selection Logic Validation

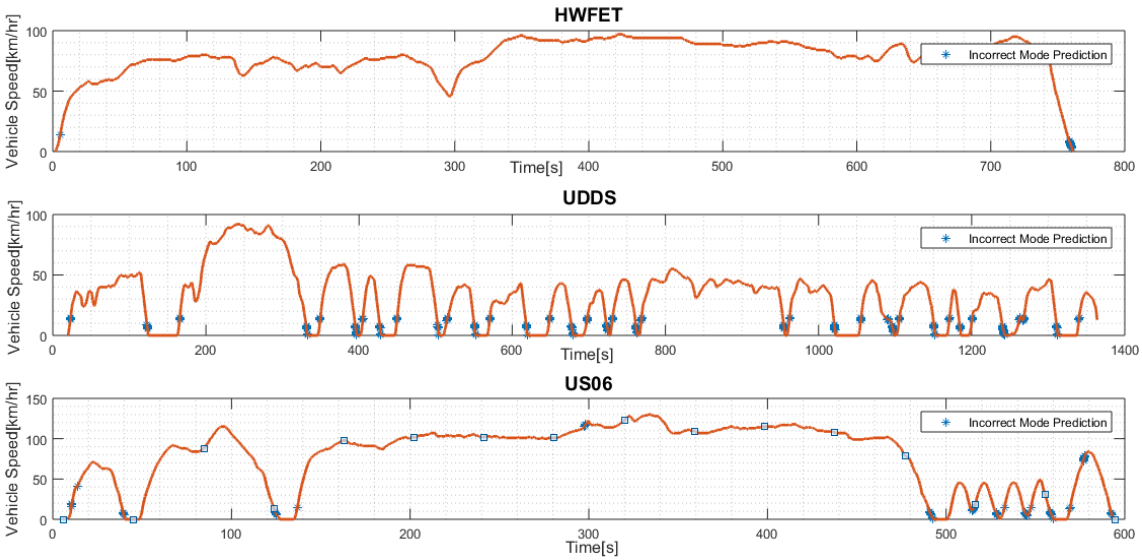

Figure 39. Mode Selection Logic Validation for all drive cycles in CD. Details in Appendix A3

Table 6. Mode Selection Logic Validation

Drive Cycle	Mode Error
HWFET	0.2
UDDS	2.25
US06	1.48

Thus, feeding the ANL inputs of vehicle speed and axle torque the logic predicts modes with errors less than 3% validating the EV mode selection logic.

The incorrect mode error points axle torque and vehicle speed are plotted on the mode selection region diagram for the three drive cycles. This is done to help identify the regions of axle torque and speed where the modes are incorrectly predicted and help us refine the logic.

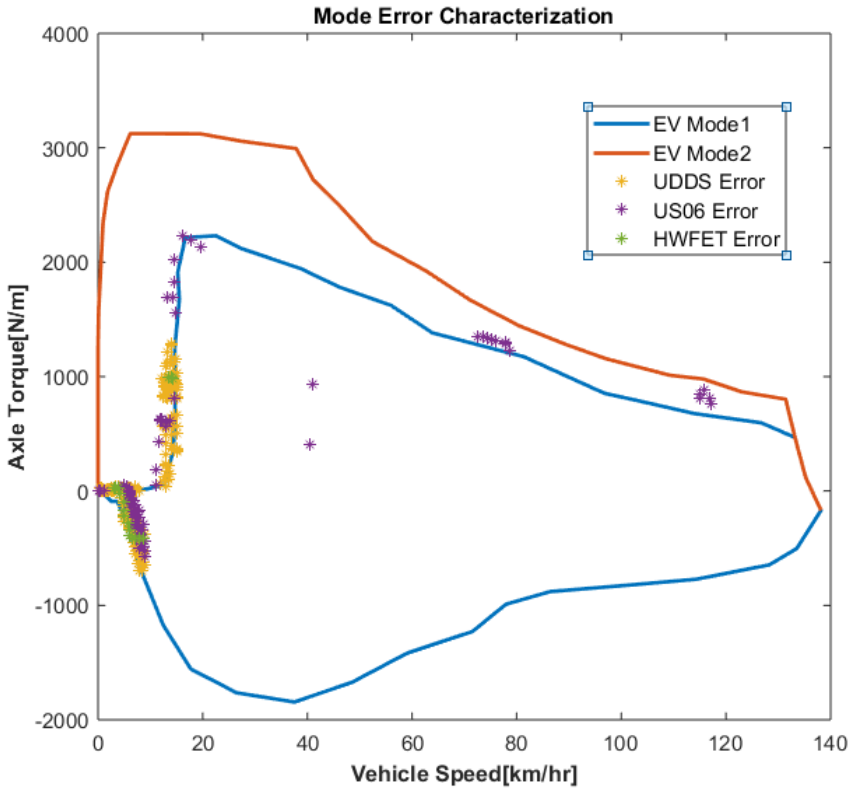

Figure 40. Mode Error Characterization

Thus, based on plotting the points it is observed that most of the error points occur on the boundary of EV mode 1 and EV mode 2. This represents the minor accuracy loss in capturing the bounding regions that contributes to this errors in mode selection. This also validates our logic which has achieved maximum accuracy and no scope for major improvement

2.8. Controller:

We used a PI controller to generate the axle torque request from the error of target and actual vehicle speed. The mode selection and torque blending logic determines the mode and corresponding motor torque based on the axle torque and vehicle speed inputs. We observe the accuracy of the controller and logic to determine the EV mode in which the vehicle operates i.e. in mode 1 or mode 2. To achieve the target drive cycle velocity and accuracy of energy consumption the following controller gains are used.

Kp=500 and Ki=200.

The controller gains were chosen such it is responsive to the system dynamics i.e. the modulate the traction forces to achieve the dynamics velocity profile. Also, care was

taken not to choose high gain values which makes the system react extremely fast to dynamics. This might cause the controller to command high traction and regenerative torque which in turn causes a highly fluctuating power demand on the battery which the battery cannot physically sustain.

3 Overall Model Validation

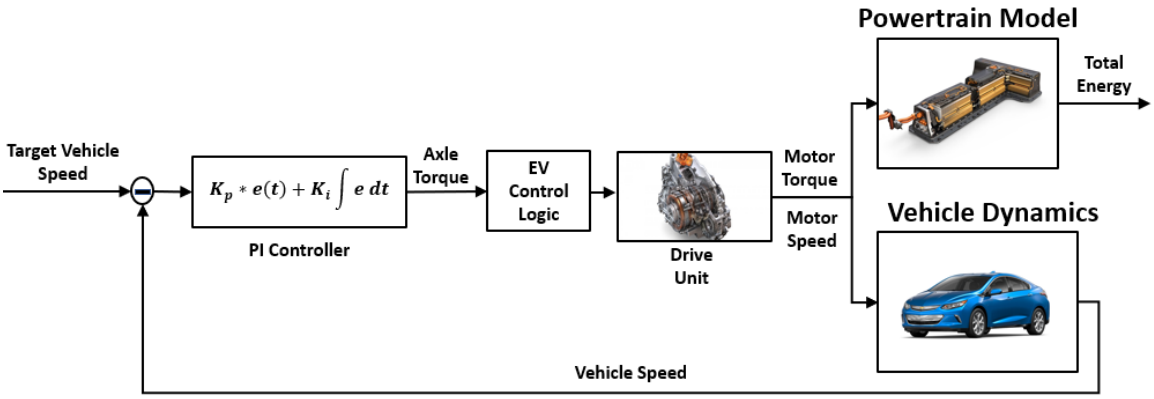

Figure 41. Overall Model Schematic

The target ANL speed is fed as input to the Chevy Volt vehicle model. The Powertrain model estimates the energy consumption for the drive cycle. The Vehicle dynamics model generates the actual vehicle speed. The PI controller generates the axle torque request based on the difference between the target and actual vehicle speed. The EV control logic which consists of the control rules for mode selection and torque blending determine the Motor A and B torques. The motor speeds are generated from the vehicle speed based on kinematic relations of the engaged planetary gearsets. The motor speeds and torque along with auxiliary energy consumption devices determine the battery power request. By integrating the supplied power by the battery over the drive cycle duration the total energy consumption is determined.

3.1 Overall Model Validation- Mode Selection

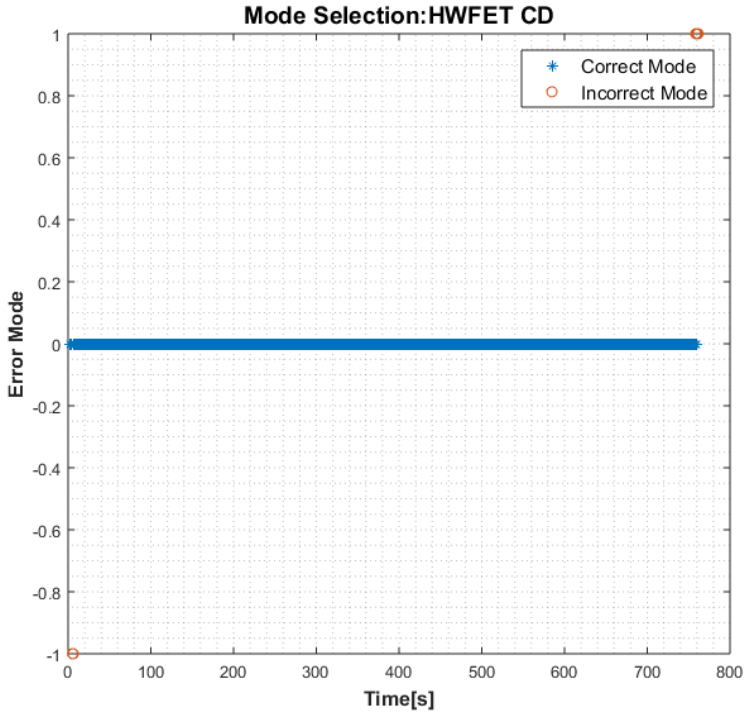

Figure 42, Mode Selection HWFET (61607018.mat). Details in Appendix A4

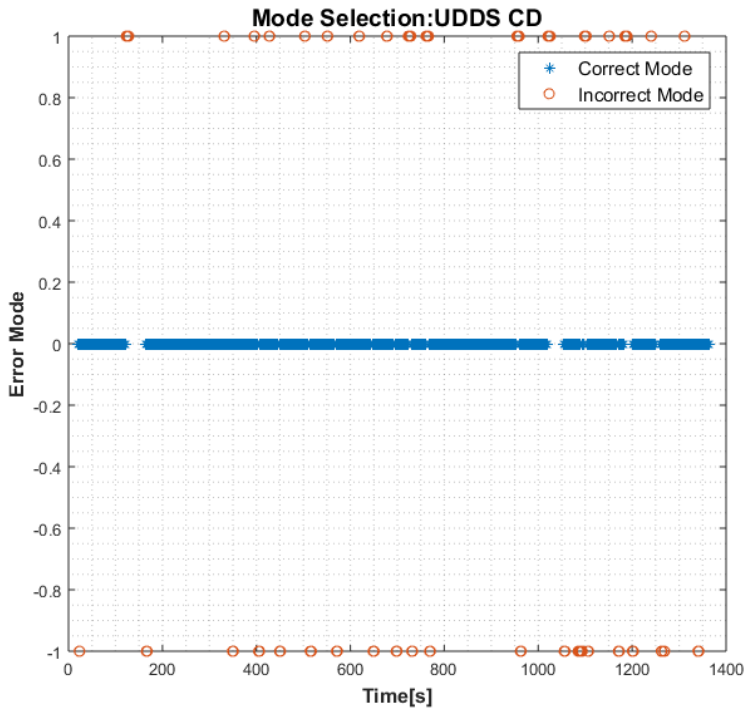

Figure 43. Mode Selection UDDS CD (61607020.mat). Details in Appendix A4

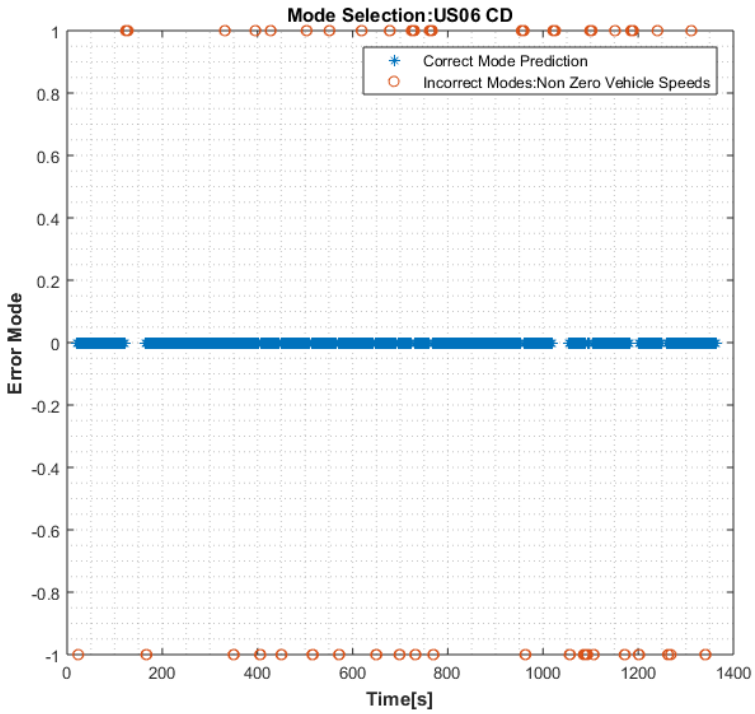

Figure 44.Mode Selection US 06 CD (61607008.mat). Details in Appendix A4

Table 7. Mode Prediction Accuracy of Controller

Drive Cycle	Mode Error (%)
HWFET	0.4
UDDS	6.8
US06	5.9

3.2 Overall Model Validation – Vehicle Velocity

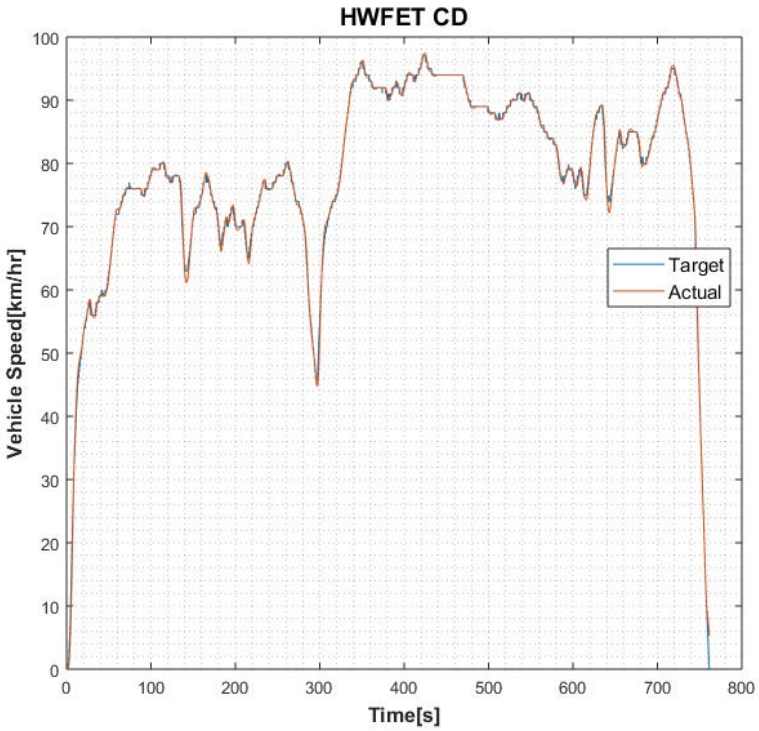

Figure 45. Vehicle Speed HWFET (61607018.mat). Details in Appendix A4

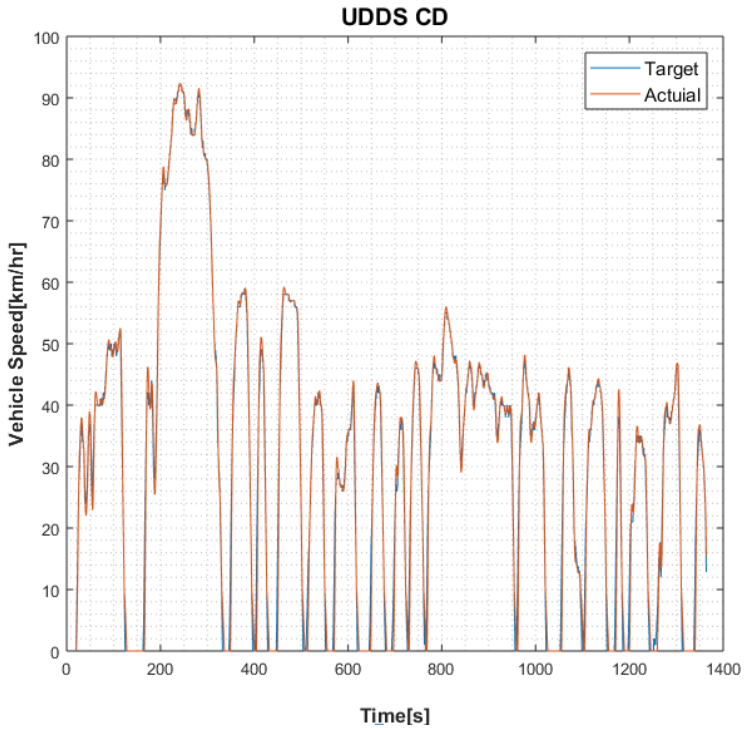

Figure 46. Vehicle Speed UDDS CD (61607020.mat). Details in Appendix A4

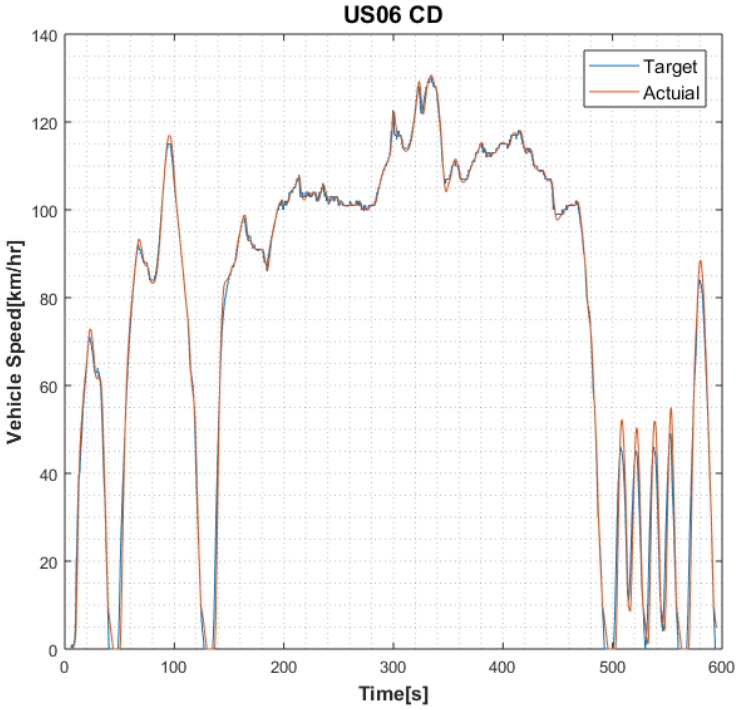

Figure 47. Vehicle Speed US 06 CD (61607008.mat). Details in Appendix A4

From the graphs we can see that PI controller makes the vehicle follow the drive cycle velocity closely.

3.3 Overall Model Validation – Battery Energy Consumption

The total energy consumed by the battery in ANL test data and model results are compared below. The experimental energy consumption total is obtained by integrating ANL values of battery current and voltage

$$Model\ Energy\ Consumption = \int V_{batt} . I_{batt} dt$$

Table 8. Comparison of overall Energy Consumption

Drive Cycle	ANL Energy Consumption	Model Energy Consumption	Error (%)
HWFET	7.85	7.57	-3.56
UDDS	5.35	5.51	+3.00
US06	8.72	8.39	-3.78

Thus, the integrated Chevy Volt vehicle model predicts total energy consumption with errors less than 5% for HWFET, UDDS and US 06 drive cycle based on the drive cycle velocity input which is our desired objective.

3.4 Error Analysis

The powertrain model uses a controller to generate its inputs. The source of errors in energy consumption is due to errors within the EV controller and within the model itself.

$$Total\ Error = EV\ Controller\ errors + Modelling\ Errors$$

The main task of the EV controller is to select modes based on axle torque request and vehicle speed inputs. The modes determine the motor torques and hence total energy consumption. A PI controller generates the axle torque request based on the model generated variable of actual vehicle speed. Hence, we lump the errors in axle torque

request as modelling errors and the only the errors in mode selection are treated as controller errors.

We feed in the ANL mode input and controller mode inputs to the powertrain model and observe the energy consumption errors and based on the difference we can deduce the individual components of controller and modelling errors

Table 9. Comparison of energy consumption errors with experimental and EV controller generated modes

Drive Cycle	Total Energy ANL Modes	Total Energy Error %	Total Energy Controller modes	Total Energy Error %
HWFET	7.57	-3.56	7.57	-3.56
UDDS	5.47	2.24	5.51	3.00
US06	8.46	-2.98	8.39	-3.78

Thus, based on the above table we can compute the absolute value of modelling and controller errors

Table 10. Individual contribution to errors from controller and model

Drive Cycle	Controller Errors (%)	Modelling Error(%)
HWFET	0	3.56
UDDS	0.8	2.24
US06	0.34	2.98

We see that the controller error is zero in HWFET case since there are no frequent mode shifts. For HWFET and UDDS cycle feeding ANL inputs help slightly improve errors in energy consumption prediction. However, for all cycles majority of errors in total energy consumption calculation come from the modelling errors

3.5 Energy Analysis

Physical subsystems and effects within the powertrain are analyzed in detail to determine their contribution to total energy consumption.

Table 11. Distribution of energy among the powertrain subsystems

Drive Cycle	Motor A [MJ]	Motor B[MJ]	Aux Pump [MJ]	Spinloss [MJ]	Total [MJ]
UDDS	0.07	4.49	0.44	0.51	5.51
HWFET	0	6.25	0.31	1.01	7.57
US06	0.03	7.12	0.34	0.9	8.39

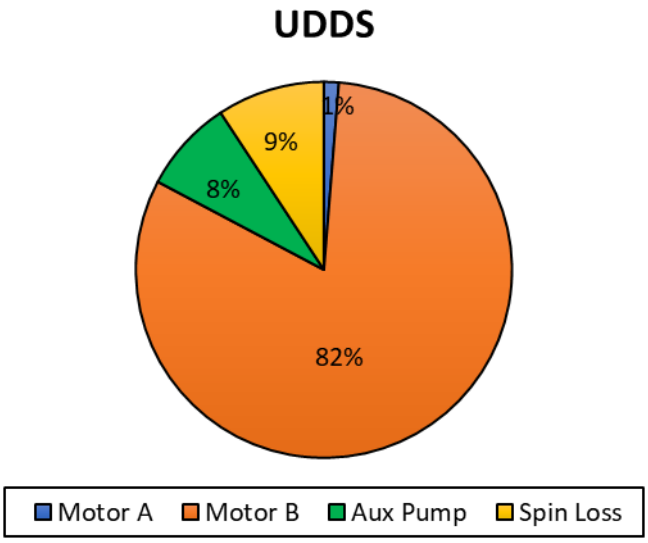

Figure 48. Energy Distribution UDDS

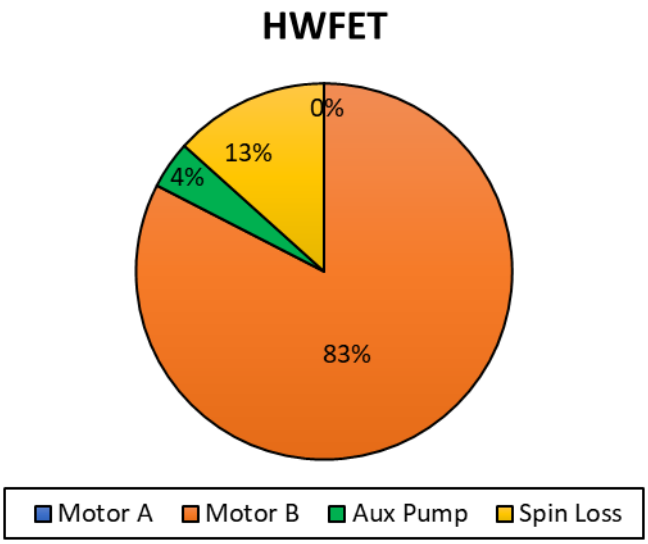

Figure 49. Energy Distribution in HWFET

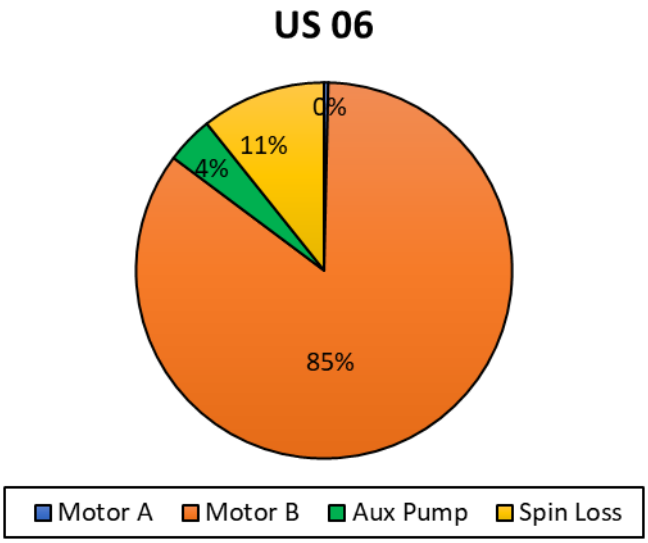

Figure 50. Energy Distribution in US 06

Thus, based on figures we can see that Motor B contributes to majority of the energy consumption. Since UDDS cycle has frequent start-stop events and low speed driving Motor A assists total requirements but its contribution is about 1%. For the high-speed drive cycles of HWFET and US06, Motor A is used sparingly and can be ignored with respect to motor A.

The auxiliary losses are much higher in UDDS cycle at 8% of total energy consumption which is nearly double compared to US06 and HWFET cycles where it stands at 4%. Since UDDS cycle has highly dynamic torque requests compared to US06 and HWFET the pump deals with greater resistances to pump the auxiliary fluid and hence consumes higher energy.

Regarding spin losses the UDDS cycle has a lower spin loss contribution is 9% whereas for the HWFET and US06 cycles are at 13% and 11%. This is due to higher transmission speeds which creates high viscous drag on the gear surfaces and hence contribute to higher spin losses.

4 Summary and Future Works:

4.1. Summary

Thus a powertrain model of Chevy Volt Gen II in EV (Charge Depleting) mode was modelled in Matlab and Simulink using parameters provided by GM. The validation of the each of the subsystem developed and overall model was carried out using ANL test data. The key highlights of the works have been summarized below:

- A dynamic model of the Li-ion battery based on the Equivalent Circuit Method was developed. Model parameters of OCV, resistances and capacitances as function of SOC and battery temperature were provided by GM.

- Static models of the Electric Motor, TPIM inverter, transmission auxiliary pump and spin losses were implemented.

- The rules implemented in Chevy Volt for EV mode selection and torque blending logic were extracted by performing a data analysis on ANL test data.

- Based on the rules a simple supervisory controller generated the motor torque and speeds from the drive velocity input.

The individual subsystem validations were presented. Finally, the overall model was validated for three test cycles in CD cases and the model predicts the total energy consumption with less than 5% error which was the objective.

4.2. Future Works

It has been observed when the battery heats above 33C the active thermal cooling kicks on to maintain the battery in the optimum temperature range. To enable active thermal cooling the HVAC compressor assists in the rejecting the heat from the battery coolant and thereby help in fast heat removal from the battery pack. The compressor action draws considerable power from the battery and there exists scope to model the battery thermal management system. Even though a simplified empirical battery cooling power equation was developed based on the limited data, through extensive vehicle testing we can characterize the compressor working and the heat transfer processes. Based on such efforts we can accurately model the energy consumption of the actively cooling system and include in calculation of energy consumption

During cold ambient conditions, the battery is required to be heated to an optimum temperature. This is to prevent the high internal resistance at low temperature to quickly

drain the battery. An electric heater is used to heat up the battery. Vehicle testing is required to determine heating power as a function of the ambient temperature and needs to be included in the energy consumption calculations.

To make the model completely independent of physical inputs apart from drive cycle velocity it is necessary to build empirical models of transmission auxiliary pump and spin losses as a function of the axle torque and vehicle speed.

References:

[1]. Office of Transportation and Air Quality U.S. Environmental Protection Agency. Draft Technical Assessment Report: Midterm Evaluation of Light-Duty Vehicle Greenhouse Gas Emission Standards and Corporate Average Fuel Economy Standards for Model Years 2022-2025".

[2]. United States Environmental Protection Agency. \Green Vehicle Guide". 2017.

[3]. Aaron Hula, Amy Bunker, Andrea Maguire, and Je_ Alson. \Light-Duty Automotive Technology, Carbon Dioxide Emissions, and Fuel Economy Trends: 1975 Through 2017". 2018.

[4]. National Research Council, 2015. Cost, Effectiveness, and Deployment of Fuel Economy Technologies for Light-Duty Vehicles. National Academies Press.

[5]. Wirasingha, S.G., Schofield, N. and Emadi, A., 2008, September. Plug-in hybrid electric vehicle developments in the US: Trends, barriers, and economic feasibility. In Vehicle Power and Propulsion Conference, 2008. VPPC'08. IEEE (pp. 1-8). IEEE.

[6] Frieske, B., Kloetzke, M. and Mauser, F., 2013, November. Trends in vehicle concept and key technology development for hybrid and battery electric vehicles. In Electric Vehicle Symposium and Exhibition (EVS27), 2013 World (pp. 1-12). IEEE.

[7] Wittmann, Jochen. "Electrification and Digitalization as Disruptive Trends: New Perspectives for the Automotive Industry?." In Phantom Ex Machina, pp. 137-159. Springer, Cham, 2017.

[8] Conlon, B., Blohm, T., Harpster, M., Holmes, A. et al., "The Next Generation “Voltec” Extended Range EV Propulsion System," SAE Int. J. Alt. Power. 4(2):2015, doi:10.4271/2015-01-1152.

[9] Jurkovic, S., Rahman, K., Patel, N. and Savagian, P., 2015. Next generation voltec electric machines; design and optimization for performance and rare-earth mitigation. SAE International Journal of Alternative Powertrains, 4(2), pp.336-342.

[10] Gao, D.W., Mi, C. and Emadi, A., 2007. Modeling and simulation of electric and hybrid vehicles. Proceedings of the IEEE, 95(4), pp.729-745.

[11] Halbach, S., Sharer, P., Pagerit, S., Rousseau, A. et al., "Model Architecture, Methods, and Interfaces for Efficient Math-Based Design and Simulation of Automotive Control Systems," SAE Technical Paper 20100241,2010, https://doi.org/10.4271/2010-01-0241.

[12] Namdoo Kim, Michael Duoba, Namwook Kim, and Aymeric Rousseau. Validating Volt PHEV model with dynamometer test data using Autonomie". SAE, Int. J. Passeng. Cars - Mech. Syst, 2013.

[13] Namwook Kim, Aymeric Rousseau, Daeheung Lee, and Henning Lohse-Busch,Thermal Model Development and Validation for 2010 Toyota Prius". SAETechnical Paper, doi:10.4271/2014-01-1784, 2014.

[14] K. B. Wipke, M. R. Cuddy, and S. D. Burch,,BADVISOR 2.1: A user-friendly advanced powertrain simulation using a combined backward/forward approach, [IEEE Trans.Vehicular Technol., vol. 48, no. 6,pp. 1751–1761, Nov. 1999.

[15] PSAT Documentation. [Online]. http://www.transportation.anl.gov/software/PSAT

[16] Powell, B.K., Bailey, K.E. and Cikanek, S.R., 1998. Dynamic modeling and control of hybrid electric vehicle powertrain systems. IEEE Control Systems, 18(5), pp.17-33.

[17] Butler, K.L., Ehsani, M. and Kamath, P., 1999. A Matlab-based modeling and simulation package for electric and hybrid electric vehicle design. IEEE Transactions on vehicular technology, 48(6), pp.1770-1778.

[18] Tremblay, O., Dessaint, L.A. and Dekkiche, A.I., 2007, September. A generic battery model for the dynamic simulation of hybrid electric vehicles. In Vehicle Power and Propulsion Conference, 2007. VPPC 2007. IEEE (pp. 284-289). Ieee.

[19] Chan, C.C., 2007. The state of the art of electric, hybrid, and fuel cell vehicles. Proceedings of the IEEE, 95(4), pp.704-718.

[20] Knauff, M.C., Dafis, C.J., Niebur, D., Kwatny, H.G., Nwankpa, C.O. and Metzer, J., 2007, May. Simulink model for hybrid power system test-bed. In Electric Ship Technologies Symposium, 2007. ESTS'07. IEEE (pp. 421-427). IEEE.

[21]. Kim, Y., Siegel, J.B. and Stefanopoulou, A.G., 2013, June. A computationally efficient thermal model of cylindrical battery cells for the estimation of radially distributed temperatures. In American Control Conference (ACC), 2013 (pp. 698-703). IEEE.

[22] Weichao Zhuang, Liangmo Wang, Xiaowu Zhang, Daofei Li, and Yin. “Mode shift map design and integrated energy management control of a multi-mode hybrid electric vehicle”. Applied Energy, 10.1016/j.apenergy.2017.07.059, 2017.

[23]. JEONG, J., Choi, S., Kim, N., Lee, H. et al., “Model Validation of the Chevrolet Volt 2016,” SAE Technical Paper 2018-01-0420, 2018, doi:10.4271/2018-01-0420.

[24] Buford, Keith, Jonathan Williams, and Matthew Simonini. Determining most energy efficient cooling control strategy of a rechargeable energy storage system. No. 2011-01-0893. SAE Technical Paper, 2011.

[25]. Zhang, Xiaoqiang, Weiping Zhang, and Geyang Lei. "A review of li-ion battery equivalent circuit models." Trans. Electr. Electron. Mater 17 (2016): 311-316.

[26]. He, Hongwen, Rui Xiong, and Jinxin Fan. "Evaluation of lithium-ion battery equivalent circuit models for state of charge estimation by an experimental approach." Energies 4, no. 4 (2011): 582-598.

Appendix A: Summary of input data and model files

A.1 Battery Model Validations:

Load TwoD_Lookup_table_parameter.mat >Load Drive Cycle Data file >Run Input_Battery.m> Run BatterySOC.slx

Figure No	Load Drive Cycle Data File	Run Model File
Figure 11	HWFET_CD_61607018.mat	BatterySOC.slx
Figure 12	UDDS_CD_61607020.mat	BatterySOC.slx
Figure 13	US06_CD_61607019.mat	BatterySOC.slx

A.2 Battery Thermal Cooling System

Load TwoD_Lookup_table_parameter.mat >Load Drive Cycle Data file >Run Input_Battery.m> Run BatteryThermalCooling.slx

Figure No	Load Data File	Run Model File
Figure 14	61607007.mat 61607008.mat 61607012.mat 61607017.mat 61607019.mat 61607031.mat	BatteryThermalCooling.slx
Figure 15	61607008.mat	BatteryThermalCooling.slx
Figure 18	61607008.mat	BatteryThermalCooling.slx

A.3 Motor Model Validation:

Load MotorTable.mat > Load Drive Cycle Data File >Run MotorInput.m> Load TwoD_Lookup_table_parameter.mat>Run Input_Battery.m>Run Motor.slx

Figure No	Load Data File	Run Model File
Figure 24	HWFET_CD_61607018.mat	Motor.slx
Figure 25	UDDS_CD_61607020.mat	Motor.slx
Figure 26	US06_CD_61607019.mat	Motor.slx

A.4 Mode Selection Logic Validation

Load Drive Cycle Data File > Run Initialize.m > Run ModeSelection.slx

Figure No	Load Data File	Run Model File
Figure 39	HWFET_CD_61607018.mat UDDS_CD_61607020.mat US06_CD_61607019.mat	ModeSelection.slx

A.5 Overall Model Validation

Load Drive Cycle Data File> Run Initialize.m > Run Volt_EV_Model.slx

Figure No	Load Data File	Run Model File
Figure 42,45	HWFET_CD_61607018.mat	Volt_EV_Model.slx
Figure 43,46	UDDS_CD_61607020.mat	Volt_EV_Model.slx
Figure 44,47	US06_CD_61607019.mat	Volt_EV_Model.slx

Appendix B: Summary of figure files

B.1 Chapter1

Figure No	Figure Files
1	Report Structure.jpg
2	LDV Production Share.jpg
3	LDV Production Share 2012 and 2017.jpg
4	MY CAFÉ 2017.jpg
5	Battery Chemistry.jpg
6	Chevy Volt Benchmark Performance.jpg

B.2 Chapter2

Figure No	Figure Files
7	Model Overview.jpg
8	Battery Circuit Diagram.vsx
9	Battery Model Schematic.vsx
10	Battery SOC Validation.jpg
11	HWFET_SOC.fig
12	UDDS_SOC.fig
13	US06_SOC.fig
14	AllCycleHVAC.fig
15,18	HVAC_Compressor_Starting_Energy.fig
16	Battery Thermal Cooling Model.jpg
17	Battery Cooling System.jpg

19	MotorAEffciency.fig
20	MotorBEfficiency.fig
21	TPIMAEff.fig
22	TPIMBEff.fig
23	Motor Model Validation.jpg
24	MotorHWFET.fig
25	MotorUDDS.fig
26	MotorUS06.fig
27	EV Mode 1.jpg
28	EV Mode 1 Lever.jpg
29	EV Mode 2.jpg
30	EV Mode 2 Lever.jpg
31	LVD.jpg
32	Aux Pump Model.jpg
33	Spinloss.jpg
34	ModeSelection.fig
35	ModeSelectionOutline.fig
36	Torque Blending Logic.jpg
37	MotorBATorqueBlendingRatio.fig
38	Mode Validation.jpg
39	ModeSubplot1.fig
40	Mode Error Characterization.jpg
41	Overall Model Schematic.jpg

B.3 Chapter3

42	HWFETMode.fig
43	UDDSMode.fig
44	US06Mode.fig
45	HWFETSpeed.fig
46	UDDSSpeed.fig
47	US06Speed.fig
48	UDDS Energy.jpg
49	HWFET Energy.jpg
50	US06 Energy.jpg